MICROWAVE DIELECTRIC RESPONSE OF NON-SPHERICAL PARTICLES BY MODULATION TECHNIQUES

Gerald Wayne Fritz

Library
Naval Postgraduate School
Monterey, California 93940

NAVAL POSTGRADUATE SCHOOL
Monterey, California

THESIS

MICROWAVE DIELECTRIC RESPONSE OF NON-SPHERICAL PARTICLES BY MODULATION TECHNIQUES

by

Gerald Wayne Fritz

Thesis Advisor: W.M. Tolles

March 1974

Approved for public release; distribution unlimited.

T158015

Microwave Dielectric Response of Non-Spherical Particles by Modulation Techniques

by

Gerald Wayne Fritz
Lieutenant, United States Navy
B.S., Virginia Polytechnic Institute, 1967

Submitted in partial fulfillment of the
requirements for the degree of

MASTER OF SCIENCE IN PHYSICS

from the

NAVAL POSTGRADUATE SCHOOL
March 1974

Thesis
F8945
c.1

Library
Naval Postgraduate School
Monterey, California 93940

ABSTRACT

A method was developed to investigate the dielectric response of non-spherical zinc oxide particles in a gaseous suspension. The method exploited a change in a microwave cavity resonance when the particles were aligned with respect to the microwave electric field. To enhance the detectability of this change, modulation techniques were employed for alignment and detection purposes.

A theory was devised to explain this method and experiments were conducted, the results of which support this theory. Investigations with the zinc oxide particles produced in these experiments indicated that the particle response demonstrated saturation and that the particles are easily aligned in an electric field strength of several hundred Volts/cm. The zinc oxide particles produced showed a relaxation frequency of approximately 56 Hz and ranged in size from approximately 2.0 to 3.5 microns in length.

TABLE OF CONTENTS

I. INTRODUCTION ---------- 10

II. THEORY ---------- 14

A. BASIC RESPONSE ---------- 14

1. Cavity Response ---------- 14

2. Perturbation by Dielectric Particles ---- 15

3. Modulation Techniques ---------- 18

B. SATURATION BEHAVIOR ---------- 24

C. RELAXATION TIME (FREQUENCY) ---------- 32

D. PARTICLE SIZE DISTRIBUTION ---------- 36

III. EXPERIMENTAL ---------- 43

A. SAMPLE PREPARATION AND PARTICULATE SUSPENSION PRODUCTION ---------- 43

B. RESONANT CAVITY DESIGNS ---------- 47

1. Rectangular – Flat Plate Reflection Cavity ---------- 47

2. Rectangular – Flat Plate Transmission Cavity ---------- 50

3. Cylindrical – Coaxial Transmission Cavity ---------- 52

C. EXPERIMENTAL APPARATUS ---------- 55

1. Reflection Cavity Equipment ---------- 55

a. Microwave Resonant Cavity ---------- 55

b. Varian Unit ---------- 55

c. Transformer and 0-500 Volt Power Supply ---------- 57

2. Reflection Cavity Block Diagram --------- 57

3. Transmission Cavity Equipment ---------- 57

a. Microwave Resonant Cavities --------- 57

b. Hewlett-Packard HP8690B Sweep Oscillator ---------- 58

c. Princeton Applied Research Lock In Amplifier/Phase Detector, Model 121 -- 59

d. Honeywell Electronik 193 Strip Recorder ---------- 60

e. Square Wave Generator ---------- 61

f. Princeton Applied Research Boxcar Integrator, Model 160 ---------- 61

4. Transmission Cavity Block Diagram -------- 62

D. VARIABLES INVESTIGATED ---------- 62

1. Cavity Response Versus Applied E-Field --- 62

2. Relaxation Frequency and Particle Size Distribution ---------- 64

3. Particle Characterization ---------- 65

a. Cavity Response Versus Temperature (ZnO Production) ---------- 65

b. Cavity Response Versus Reactant Gas Flow Rates ---------- 65

IV. RESULTS AND DISCUSSION ---------- 66

A. BASIC RESPONSE ---------- 67

B. DERIVATIVE RESPONSE ---------- 76

C. SATURATION BEHAVIOR ---------- 78

D. RELAXATION TIME (FREQUENCY) ---------- 81

E. PARTICLE SIZE DISTRIBUTION ---------- 86

F. PARTICLE CHARACTERIZATION ---------- 89

1. Response Versus Temperature (ZnO Production) ---------- 89

2. Reactant Gas Flow Rates ---------- 89

V. SUMMARY AND CONCLUSIONS ---------- 96

BIBLIOGRAPHY ---------- 100

INITIAL DISTRIBUTION LIST ---------- 102

FORM DD 1473 ---------- 103

LIST OF TABLES

Table I	Values of $f(E) = \langle \cos^2\theta - 1/3 \rangle$ and Derivative of f(E) ----------	29
Table II	Value of $F(E) = \langle 1/3 - \cos^2\theta \rangle$ and Derivative of F(E) ----------	30
Table III	Predicted Relaxation Times and Frequencies for ZnO Cylinders ----------	37
Table IV	Calculated Ratio of Peak Imaginary/Peak Real Response for a Given Value of σ -------	41
Table V	Comparison of Determined Particle Sizes for Investigations Performed (ZnO Particles) ----------	98

LIST OF ILLUSTRATIONS

Figure		
1.	Particle Alignment Process	18
2.	Cavity Resonance (Random Alignment)	19
3.	Cavity Resonance (Forced Alignment)	19
4.	Cavity Response (Modulation Potential Applied)	20
5.	Demodulated Response	20
6.	Equivalent Circuit for Transmission Cavity	22
7.	Response Line Shape Dependence on Percent Real Sample Response	24
8.	Predicted Response, f(E), and $\partial f(E)/\partial A$ versus A	31
9.	General Form for $1/1 - i\omega\tau$ for Single Valued τ	38
10.	Predicted Response versus Frequency for Different σ Values	42
11.	Particulate Production	46
12a,b	SEM Photographs of Collected Samples of ZnO Particles	46
13.	Reflection Rectangular Cavity and Microwave Mode Pattern	48
14.	Transmission Rectangular Cavity	51
15.	Cylindrical Coaxial Cavity and Microwave Mode Pattern	53
16.	Reflection Cavity Apparatus Block Diagram	56
17.	Transmission Cavity Apparatus Block Diagram	63
18.	In Phase and Out of Phase Response for ZnO	73
19.	Effect of ZnO (0.05 Mole % In) Core Aging on In Phase Response	75
20.	Derivative Response from Sine Wave Modulation	77

21. Response of 31.7 Hz Square Wave Modulation Versus Applied E-Field ---------- 80

22. Integrated Response of 31.7 Hz Sine Wave Modulation Versus Applied E-Field ---------- 82

23. In Phase and Out of Phase Response Versus Log_{10} Frequency ---------- 84

24. SEM Photographs of Collected Samples of ZnO Produced (a) during Relaxation Frequency Investigation and (b) during Boxcar Integrator Investigation ---------- 85

25. Boxcar Integrator Response ---------- 87

26. Relative Response Versus ZnO Production Temperature ---------- 90

27. Particle Length Versus ZnO Production Temperature ---------- 91

28. SEM Photographs of ZnO Particles Produced at Temperatures from 1000° to 1275°C ---------- 92

29. Response Versus Hydrogen Flow Rate ---------- 93

30. Response Versus Oxygen Flow Rate ---------- 95

ACKNOWLEDGEMENT

The author would like to acknowledge the invaluable assistance and guidance provided by Professor William Tolles. Without his insight in overcoming what appeared to be insurmountable problems, especially in cavity design, this study could not have been accomplished.

Deserving a special note of thanks is Mr. Robert Sanders who assisted in constructing the experimental apparatus and provided the technical expertise on unfamiliar components.

I. INTRODUCTION

Dielectric behavior as a method of studying molecular systems has been a topic of research since 1912 when P. Debye first introduced a theory for the interpretation of the dielectric constant and loss associated with un-ionized materials. References 1 and 2 contain the basic theories presented by Debye and Fröhlich in order to explain dielectric properties. The basic dielectric response arises from the charge separation induced by electric fields and is described in general by the dielectric constant tensor. Dielectric saturation and dispersion are phenomena directly associated with the total polarizability of a material. Saturation effects result from a limitation of the polarizability of a material when subjected to strong electric fields. Dispersion is a function of the frequency of the applied field and is a result of the relaxation of the orientational contribution to the total polarizability.

Dielectric properties of molecular systems in the gaseous, liquid, or solid state have been characterized for a large number of materials and the response mechanisms are understood. For these molecular systems, the effects of saturation and dispersion are usually observed in fields of approximately 10^5 Volt/cm (saturation) and 10^{12} Hz (dispersion). These effects are discussed in Refs. 3 and 4.

Methods used to obtain dielectric constants include a comparison of capacitance measurements for static or low

frequencies, and microwave methods for high frequencies [3,4]. Microwave methods involve the measurement of a resonant cavity shift and attenuation when a dielectric material is introduced into the cavity. The material is generally placed at a point of maximum electric field strength. This procedure insures the greatest attenuation and frequency shift.

Solid non-spherical dielectric particles suspended in a gas should also exhibit dielectric behavior and therefore be characterized by dielectric methods. However, until recently little attention has been given to a characterization of this behavior or to methods developed for their study. Microwave measurement techniques have been applied to dielectric studies previously and should be useful in particulate suspension studies.

The application of an electric field to particles having an anisotropic polarizability tensor tends to align these particles with the field. This fact suggests a technique for modulating the particle alignment and studying properties of such systems. Modulation techniques when applied to a system improve the overall detectability of a small change in a material property such as a microwave frequency shift and attenuation.

The primary objective of this study was to develop a means to investigate dielectric non-spherical particulate suspensions utilizing dielectric and microwave methods for characterization and detection purposes. The basic concept

involved the introduction of a particulate suspension into a resonant microwave cavity where an impressed electric field forced particle alignment with respect to the microwave electric field. The particle alignment resulted in a change in a microwave cavity resonance frequency and Q. Modulation techniques were then employed for particle alignment and detection purposes.

Representative studies of recent investigations in the area of non-spherical particles are presented as an introduction to previously utilized methods. Atlas, Kerker, and Hitschfeld in Ref. 5 investigated the effects of non-spherical atmospheric particles on the returned radar echo from rain and snow. Jones in Ref. 6 investigated the increase in IR emissivity due to the elongation of suspended carbon particles and the effects of "streaming birefringence" and/or electric fields. The tendency of electric fields to align the particles led to an increase or decrease in emissivity depending on particle orientation relative to the incident IR radiation. Vogel, Circle, and Powell in Ref. 7 investigated the optical character of irregularly shaped zinc oxide particles using an angular scanning spectropolarimeter and back scattering.

Section II develops and expands a theory for the basic dielectric response, saturation behavior, and relaxation phenomena expected for general non-spherical suspended dielectric particles. Section III provides a description of the method used for particulate suspension production, the

experimental apparatus, and the evolution of microwave cavity designs used to observe and record the response. Section IV is a discussion of the results obtained from a suspension of zinc oxide particles illustrating the basic response, saturation behavior, relaxation frequency determination, and particle size distribution. Section IV also contains the results obtained as a characterization of the sensitivity of the response exhibited by zinc oxide to varying conditions of reactant gas flow rates and temperature of zinc oxide production.

The methods currently in use in the study of highly dispersed aerosols (HDA), listed in Ref. 8, include light scattering and precipitation measurements to determine either an average particle size or a distribution of particle sizes. The methods employed here to obtain a response related to dielectric behavior provide a means to investigate particulate suspensions without reliance on either particle magnification or precipitation. By an investigation of saturation and relaxation behavior, particle size and size distributions can be determined. For these reasons the following study should be of interest in aerosol physics research, pollution studies, and in the expansion of scattering and nucleation theory.

II. THEORY

The following theory for the response exhibited by non-spherical dielectric particles was developed as a general explanation of the basic response and predicted dielectric behavior associated with the phenomena of saturation and relaxation in an electric field. The theory was expanded to include modulation techniques employed to enhance the detectability of the response. A development of a method to determine the size distribution of suspended particles by comparison of the real (in phase) and imaginary (90° out of phase) response is also included.

Although the supporting experimental investigations dealt exclusively with the response exhibited by zinc oxide (ZnO) particulate suspensions, the theory should apply to other dielectric materials as long as the assumption of a cylindrical particle shape is valid. Table III which predicts relaxation frequencies for a range of particle sizes applies only to ZnO.

A. BASIC RESPONSE

1. Cavity Resonance

By a consideration of the geometrical dimensions of a cavity, the resonant frequencies for a given mode can be determined. For a rectangular geometry the resonant wave length, λ , for a given mode, TE n_x, n_y, n_z, is given by:

$$\frac{1}{\lambda^2} = \frac{n_x^2}{4L_x^2} + \frac{n_y^2}{4L_y^2} + \frac{n_z^2}{4L_z^2} \qquad (1)$$

where n_x, n_y, n_z are the number of half wave lengths for the given cavity dimensions and L_x, L_y, L_z are the cavity dimensions. For a cylindrical, coaxial geometry, Beringer in Ref. 9, developed an equation for resonant TE modes as

$$\lambda^2 = \frac{4}{\left(\frac{2\,\chi_{\ell m}}{\pi\, D}\right)^2 + \left(\frac{n}{L}\right)^2} \qquad (2)$$

where $\chi_{\ell m}$ = roots of $J'_\ell(x)N'_\ell(\eta x) = J'_\ell(\eta x)N'_\ell(x)$ and J'_ℓ and N'_ℓ are Bessel functions of the first and second kind, $\eta = \frac{b}{a}$ (b = inside cylinder radius, a = D = outside cylinder radius), n = number of half wave lengths along cavity length, and L = cavity length. Charted values of $\chi_{\ell m}$ and $\chi_{\ell m}(1-\eta)$ versus η for each resonant mode[9], remove the cumbersome procedure of solving for $\chi_{\ell m}$ for each value of η.

2. Perturbation by Dielectric Particles

When an object is introduced into a microwave cavity, its presence will perturb the cavity by causing a shift in the resonant frequency and/or a decrease in the quality factor, Q, for the cavity by attenuating to some extent the cavity microwave fields. The exact type of perturbation which a particle causes depends on the particle susceptibility, geometry, location and orientation within the cavity.

To illustrate these perturbations, first consider a thin metallic needle. If the needle is suspended in the cavity and is free to assume a random orientation, the resonant frequency will change as the needle's orientation is

changed with respect to the microwave E-field. When the needle is perpendicular to the E-field there will be little if any frequency shift. The amount of this shift increases as the needle rotates to a more parallel alignment and reaches a maximum when the needle aligns parallel to the E-field. Ginzton in Ref. 10 utilizes a needle-shaped metallic object suspended in a cavity to determine the orientation of the electric field.

If a dipole (multipole) moment can be induced in a dielectric material, then the induced dipole will cause a cavity response similar to that described for the metallic needle. In addition to this response, if the dielectric being introduced has a complex electric susceptibility, $\chi_e = \chi_e' - j\,\chi_e''$, then the material will not only cause a resonance frequency shift but will also attenuate the microwave fields. By extending the development given by Lax and Button in Ref. 11, the extent of the frequency shift, $\Delta\omega_o$, and the attenuation, $\Delta(1/Q_e)$ are given by

$$\frac{\Delta\omega_o}{\omega_o} = -\frac{\int_{Vol} \chi_e'(x,y,z)\, E^2(x,y,z)\, dxdydz}{2 \int_{Vol} E^2(x,y,z)\, dxdydz} \qquad (3)$$

and

$$\Delta\left(\frac{1}{Q_e}\right) = \frac{\int_{Vol} E^2(x,y,z)\, \chi_e''(x,y,z)\, dxdydz}{\int_{Vol} E^2(x,y,z)\, dxdydz} \qquad (4)$$

where the volume is the volume of the perturbing material introduced. The problem remains to induce the dipole moment and observe the response.

If rod-like (needles) dielectric particles are subjected to an electric field, a dipole moment will be induced in the particles as the field forces a migration of charge or charge separation and the resultant torque on these particles will tend to align the particles along the field lines in a lower energy configuration. The energy stored in the particles because of the forced charge migration is dependent on the dipole moment, p, and the electric field strength, E. Pauling and Wilson in Ref. 12 give the energy stored in a polarizable material in terms of α, the polarizability, and E as:

$$W = -\frac{1}{2}\alpha E^2 \quad . \tag{5}$$

Figure 1 depicts the particle alignment process as discussed above.

If a potential could be applied across a microwave cavity, parallel to the microwave E-field and suspended non-spherical dielectric particles introduced into the cavity then the aligned dielectric particles would show a frequency shift relative to the resonant frequency observed for randomly oriented particles. If the particles are lossy, an attenuation of the microwave field will also be observed. The microwave cavities described in Section III B are designed so that a

potential may be applied with the geometry necessary to observe this response in the cavity.

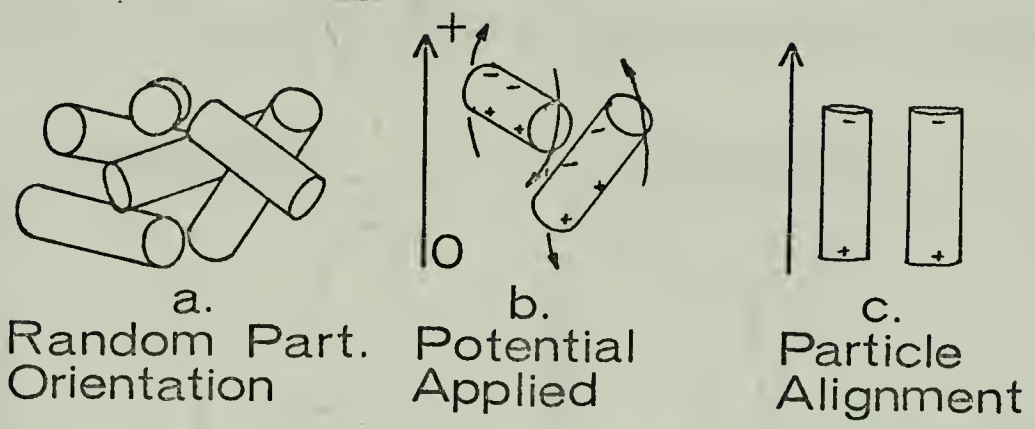

ALIGNMENT PROCESS
Figure 1

3. Modulation Techniques

The resultant resonance frequency shift and cavity attenuation could be measured by static means applying the methods outlined by Ginzton and Lax and Button; however, if the particles are in a suspension and dynamically changing, these phenomena become extremely difficult to observe. In order to enhance the detection and measurement of this response, modulation techniques can be applied.

Basically the techniques involve the application of an electric field as a sine or square wave variation in order to modulate the particle alignment with respect to the cavity mode microwave electric field. In conjunction with the

modulation of the particle alignment, the microwave frequency is swept across the cavity resonance. Figures 2 and 3 show the two cavity resonance conditions for an aligned and random orientation of particles with a complex dielectric constant.

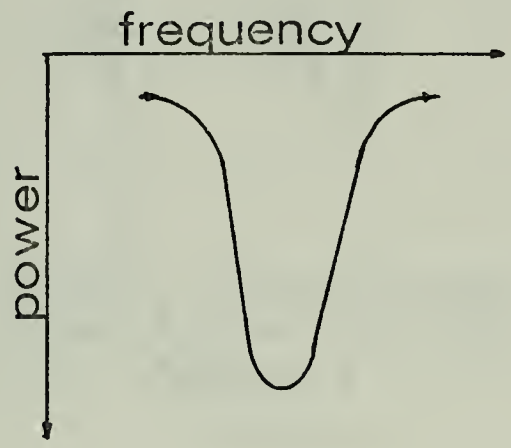

Cavity Resonance
(Random Alignment)
Figure 2

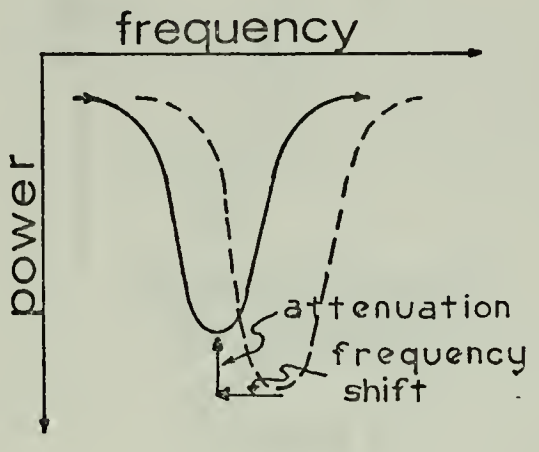

Cavity Resonance
(Forced Alignment)
Figure 3

If the applied E-field is modulated at a given frequency, the cavity response will shift from one resonant condition to the other at the modulation frequency and, if a detector is set to detect and amplify the presence of this modulation in the transmitted microwave signal, then a measure of the response can be obtained. The magnitude of this response depends on the difference between the two resonance conditions and varies as the frequency is swept over the resonant mode. Figures 4 and 5 represent the modulation between the two resonance conditions and the detected (demodulated) amplitude of the difference between the resonance conditions.

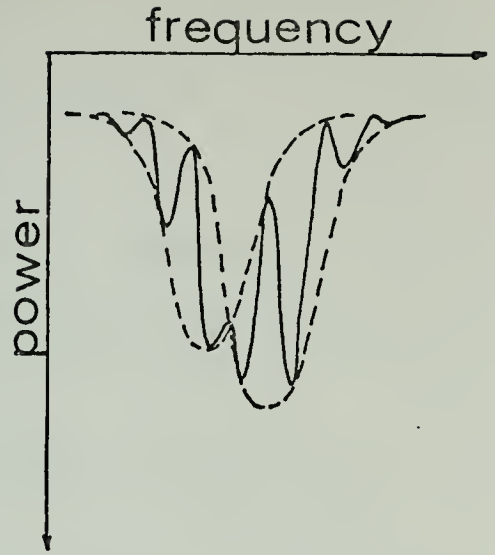

Cavity Resonance (Modulation Potential Applied)

Figure 4

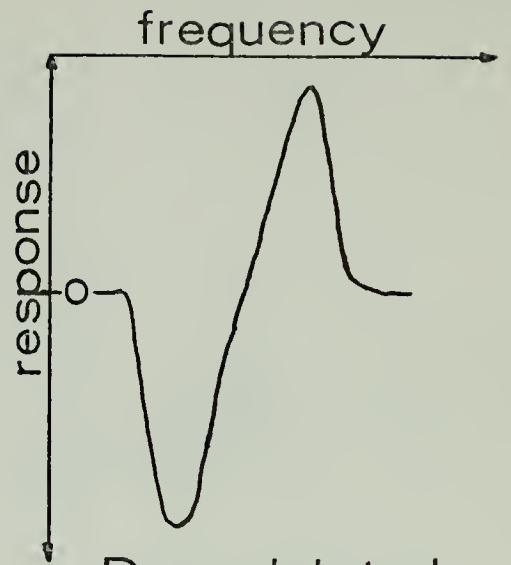

Demodulated Response

Figure 5

If the modulation is applied as a sine wave then the change in the detected response as the applied potential is changed can be detected and gives rise to a derivative type response with respect to the applied potential.

To better define the response illustrated in figure 5, consider a transmission cavity and a material with a complex dielectric constant. Ditchfield in Ref. 13 developed an expression for the transmission coefficient of a transmission cavity from an equivalent circuit, figure 6, as

$$\tau(\omega) = \frac{4\beta_1\beta_2}{(1+\beta_1+\beta_2)^2 + Q_u^2\left(\frac{\omega}{\omega_o} - \frac{\omega_o}{\omega}\right)^2} \qquad (6)$$

where

$$\beta_1 = \frac{n_1^2 R_G}{r} \quad , \quad \beta_2 = \frac{n_2^2 R_D}{r} \quad , \quad Q_u = \frac{\omega_o L}{r}$$

If Q_u is high and letting β_1 & $\beta_2 << 1$
and $\omega = \omega_o + \Delta\omega$ then:

$$\tau(\omega) \simeq \frac{4K'/r^2}{1 + 4Q_u^2 \frac{\Delta\omega^2}{\omega_o^2}} \quad , \quad K' = n_1^2 n_2^2 R_G R_D$$

Note that the width, δ , of the resonance is

$$\frac{4Q_u^2}{\omega_o^2} \left(\frac{\delta}{2}\right)^2 = 1 \quad \text{or} \quad \delta = \frac{\omega_o}{Q}$$

The width of the resonance is also proportional to r and the "height" of the resonance is proportional to $1/r^2$,

if $x \equiv 2 Q_u \frac{\Delta\omega}{\omega_o} = \frac{2\Delta\omega}{\delta}$

and $K = \frac{4K'}{L^2}$

$$\tau(\omega) = \frac{K/\delta^2}{1 + x^2} \qquad (7)$$

If the experimental apparatus is designed to respond or measure a change in $\tau(\omega)$ at a given frequency, then when either δ or ω_o changes there will be a change in the detected signal as

$$\frac{\partial \tau}{\partial \omega_o} = \frac{\partial x}{\partial \omega_o} \frac{\partial \tau}{\partial x} = \frac{2K}{\delta^3} \frac{x}{(1+x^2)^2}$$

$$\frac{\partial \tau}{\partial \delta} = -\frac{K}{\delta^3} \frac{1}{(1+x^2)^2}$$

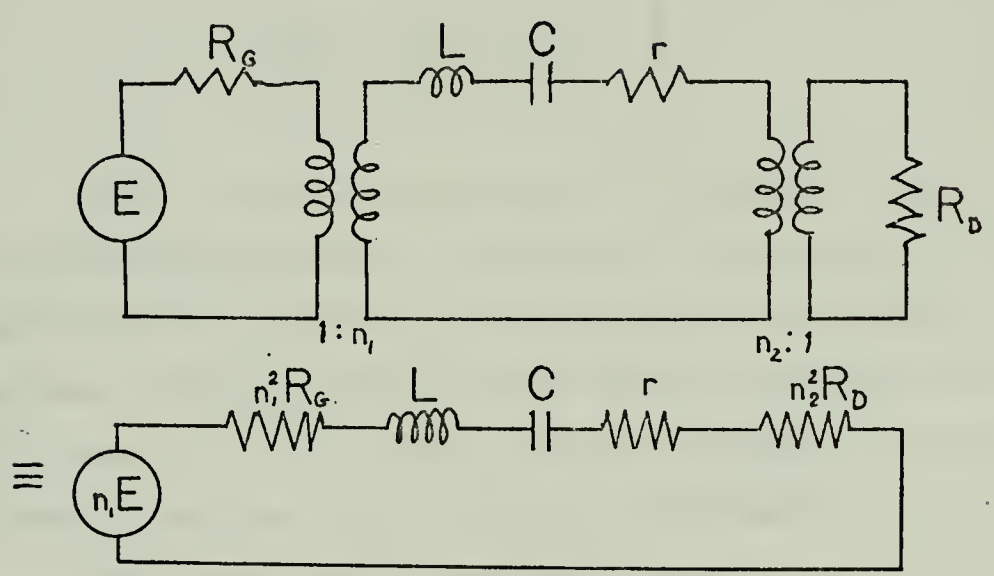

EQUIVALENT CIRCUIT FOR TRANSMISSION CAVITY

Figure 6

In general if the dielectric constant has both real and imaginary components then:

$$\Delta\tau = \frac{\partial\tau}{\partial\omega_o}\Delta\omega_o + \frac{\partial\tau}{\partial\delta}\Delta\delta$$

$$= \frac{K}{\delta^3}\left[\frac{2x}{(1+x^2)^2}\Delta\omega_o - \frac{1}{(1+x^2)^2}\Delta\delta\right] \qquad (8)$$

Let the value of $\Delta\delta = (1-R)\Delta\omega_o$ and $\Delta\omega_o = -R\,\Delta\omega_o$ where R is a number between 0 and 1 representing the percentage frequency shift ($\Delta\omega_o$) present in the detected signal. Making these substitutions gives

$$\Delta\tau = -\frac{K\Delta\omega_o}{\delta^3}\left[\frac{R(2x-1)+1}{(1+x^2)^2}\right] \qquad (9)$$

This function when plotted for different values of R shows the dependence of the shape of the response on the magnitude of the real ($\Delta\omega_o$) and imaginary (δ) sample responses. Figure 7 depicts this function plotted for a wholly real (R = 1.0), equal real and imaginary (R = 0.5), and wholly imaginary (R = 0.0) type responses.

This development provides a means of determining the approximate percentage real, and imaginary, response exhibited by the sample.

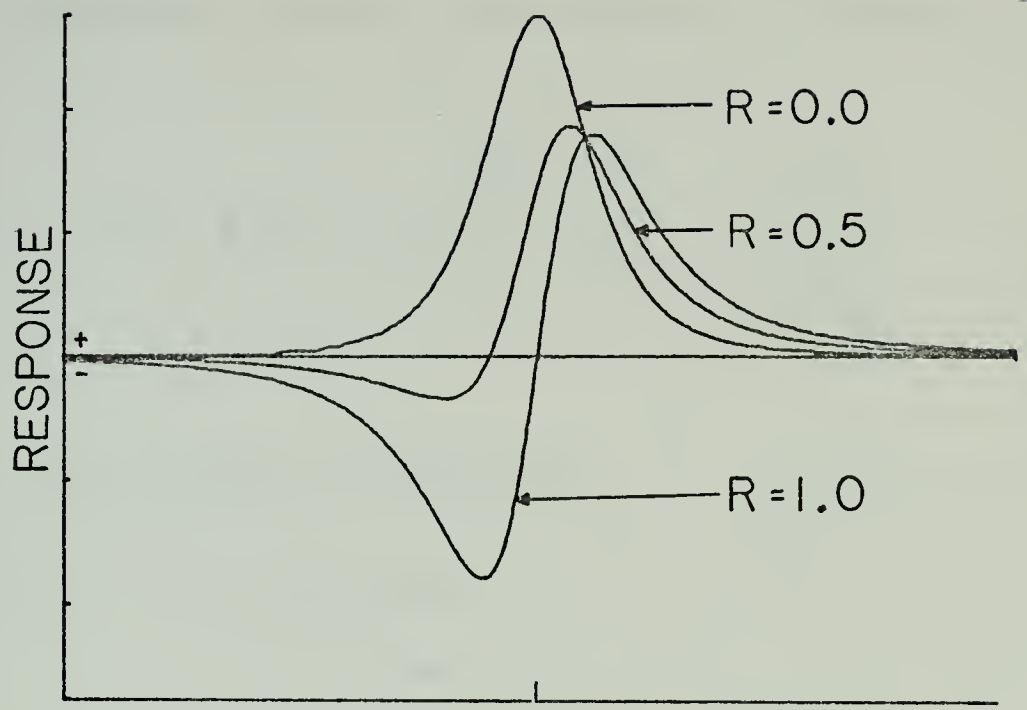

FIGURE 7

B. SATURATION BEHAVIOR

If the magnitude of the response tends to approach a constant value as the applied field is increased (i.e. the rate of change of the response as the applied field is increased tends to zero) the response is said to saturate [4].

Since the polarizability α is in reality a tensor quantity, equation (5) can be rewritten in vector notation as:

$$W = -\frac{1}{2}\ \vec{E}\cdot\vec{\vec{\alpha}}\cdot\vec{E} \qquad (10)$$

The polarizability tensor is assumed to be symmetric and diagonalized by using the appropriate orthogonal transformation. In matrix form equation (10) becomes:

$$W = -\frac{1}{2}\,(E_x\ E_y\ E_z)\begin{pmatrix}\alpha_{xx} & 0 & 0\\ 0 & \alpha_{yy} & 0\\ 0 & 0 & \alpha_{zz}\end{pmatrix}\begin{pmatrix}E_x\\ E_y\\ E_z\end{pmatrix} \quad .$$

If E is in the x-z plane then

$$E_x = E\sin\theta$$

$$E_z = E\cos\theta$$

where

θ = angle with respect to z axis.

Then

$$W = -\frac{1}{2}\,(\alpha_{xx}E^2\sin^2\theta + \alpha_{zz}E^2\cos^2\theta) \quad .$$

Furthermore if it is assumed that $\alpha_{zz} >> \alpha_{xx}$ (α_{zz} along particle length) then

$$W \cong -\frac{1}{2}\,\alpha_{zz}E^2\cos^2\theta \qquad (11)$$

In order to estimate the average response of these particles at a given E-field strength it is necessary to calculate the average induced polarization along the direction of the applied E-field. Assuming that a Boltzmann energy distribution exists, the average particle response as a function of E, f(E), will be proportional to the average particle alignment. The average particle alignment is given by $\langle \cos^2\theta \rangle$,

$$\langle \cos^2\theta \rangle = \frac{\int_0^{\pi} \cos^2\theta \exp\{\frac{\alpha_{zz}\cos^2\theta\, E^2}{2\,k\,T}\} \sin\theta\, d\theta}{\int_0^{\pi} \exp\{\frac{\alpha_{zz}\cos^2\theta\, E^2}{2\,k\,T}\} \sin\theta\, d\theta}$$

however for zero E field

$$\langle \cos^2\theta \rangle = \frac{\int_0^{\pi} \cos^2\theta \sin\theta\, d\theta}{\int_0^{\pi} \sin\theta\, d\theta} = \frac{1}{3} \quad .$$

Therefore to calculate the average particle response it is necessary to calculate $\langle \cos^2\theta - \frac{1}{3} \rangle$:

$$f(E) = \langle \cos^2\theta - \tfrac{1}{3} \rangle = \frac{\int_0^{\pi} (\cos^2\theta - \frac{1}{3}) \exp\{\frac{\alpha_{zz}E^2\cos^2\theta}{2kT}\} \sin\theta \, d\theta}{\int_0^{\pi} \exp\{\frac{\alpha_{zz}E^2\cos^2\theta}{2kT}\} \sin\theta \, d\theta} \qquad (12)$$

using $A^2 \equiv \frac{\alpha_{zz}E^2}{2kT}$

substituting $x = \cos\theta$, $dx = -\sin\theta \, d\theta$ and integrating by parts

$$f(E) = \frac{1}{2A^2} \left(\frac{1}{\int_0^1 \exp\{A^2(x^2-1)\} \, dx} - 1 \right) - \frac{1}{3} \qquad (13).$$

Let $I = \frac{1}{\int_0^1 \exp\{A^2(x^2-1)\} \, dx}$.

This f(E) then becomes the average particle alignment; however, the average response as the particles are deflected away from an aligned configuration becomes

$$F(E) = \langle \tfrac{1}{3} - \cos^2\theta \rangle = \frac{\int_0^{\pi} (\frac{1}{3} - \cos^2\theta) \exp\{\frac{-\alpha_{zz}E^2\cos^2\theta}{2kT}\} \sin\theta \, d\theta}{\int_0^{\pi} \exp\{\frac{-\alpha_{zz}E^2\cos^2\theta}{2kT}\} \sin\theta \, d\theta}$$

The solution follows exactly the same development as for equation 12 except that A now becomes -A and

$$F(E) = \frac{1}{3} - \frac{1}{2A^2}\left(\frac{1}{\int_0^1 \exp\{-A^2(x^2-1)\}\,dx} - 1\right) \qquad (14)$$

To determine the derivative df(E)/dE first determine $\frac{\partial f(E)}{\partial A}$ then

$$\frac{df(E)}{dE} = \frac{\partial f(E)}{\partial A}\,\frac{\partial A}{\partial E}$$

$$\frac{\partial A}{\partial E} = \frac{\alpha_{zz}}{2kT} = \text{a constant}$$

and $$\frac{\partial f(E)}{\partial E} = \frac{I(2A^2-1) - I^2 + 2}{2A^3} \qquad (15).$$

Using Simpson's Rule for Numerical Integration, a program was developed for the IBM 360 computer to evaluate $\left[\int_0^1 \exp\{A^2(x^2-1)dx\}\right]^{-1}$. A table of values for this integral was developed for increments in A of 0.1. Also corresponding values for f(E) and $\frac{\partial f(E)}{\partial A}$ were developed for the same incremental values of A. (Tables I and II).

TABLE I

Values of $f(E) = \langle \cos^2\theta - \frac{1}{3} \rangle$

A	0.0	0.1	0.2	0.3	0.4	0.5	0.6	0.7	0.8	0.9
0.0	0.0	0.00089	0.00357	0.00807	0.01443	0.02273	0.03304	0.04544	0.06000	0.07681
1.0	0.09590	0.11726	0.14083	0.16646	0.19390	0.22281	0.25272	0.28311	0.31338	0.34296
2.0	0.37129	0.39794	0.42258	0.44502	0.46521	0.48319	0.49911	0.51314	0.52550	0.53639
3.0	0.54602	0.55456	0.56216	0.56898	0.57510	0.58064	0.58566	0.59024	0.59443	0.59827
4.0	0.60180	0.60506	0.60807	0.61087	0.61346	0.61588	0.61813	0.62023	0.62220	0.62404
5.0	0.62577	0.62740	0.62893	0.63037	0.63173	0.63301	0.63422	0.63537	0.63646	0.63749
6.0	0.63847	0.63940	0.64029	0.64113	0.64193	0.64270	0.64343	0.64413	0.64479	0.64543
7.0	0.64604	0.64662	0.64718	0.64772	0.64823	0.64872	0.64920	0.64965	0.65009	0.65051
8.0	0.65091	0.65130	0.65168	0.65204	0.65239	0.65272	0.65305	0.65336	0.65366	0.65396
9.0	0.65424	0.65451	0.65478	0.65503	0.65528	0.65552	0.65575	0.65597	0.65619	0.65640

Derivative of f(E)

A	0.0	0.1	0.2	0.3	0.4	0.5	0.6	0.7	0.8	0.9
0.0	0.0	0.01781	0.03582	0.05423	0.07320	0.09289	0.11338	0.13470	0.15678	0.17943
1.0	0.20229	0.22483	0.24633	0.26586	0.28242	0.29493	0.30245	0.30430	0.30020	0.29039
2.0	0.27557	0.25686	0.23559	0.21313	0.19069	0.16923	0.14942	0.13160	0.11591	0.10227
3.0	0.09054	0.08049	0.07189	0.06452	0.05818	0.05269	0.04792	0.04374	0.04006	0.03680
4.0	0.03391	0.03132	0.02900	0.02691	0.02502	0.02330	0.02175	0.02033	0.01904	0.01785
5.0	0.01676	0.01576	0.01484	0.01399	0.01321	0.01248	0.01180	0.01118	0.01060	0.01005
6.0	0.00955	0.00908	0.00864	0.00822	0.00784	0.00748	0.00714	0.00682	0.00652	0.00623
7.0	0.00597	0.00572	0.00548	0.00526	0.00504	0.00484	0.00466	0.00448	0.00431	0.00415
8.0	0.00399	0.00385	0.00371	0.00358	0.00346	0.00335	0.00323	0.00313	0.00303	0.00294
9.0	0.00285	0.00276	0.00268	0.00261	0.00254	0.00247	0.00241	0.00235	0.00230	0.00224

TABLE II

Values of $F(E) = \langle \frac{1}{3} - \cos^2\theta \rangle$

A	0.0	0.1	0.2	0.3	0.4	0.5	0.6	0.7	0.8	0.9
0.0	0.0	0.00089	0.00354	0.00793	0.01400	0.02168	0.03086	0.04141	0.05318	0.06599
1.0	0.07963	0.09387	0.10848	0.12321	0.13784	0.15215	0.16594	0.17907	0.19142	0.20292
2.0	0.21352	0.22323	0.23206	0.24005	0.24727	0.25377	0.25962	0.26489	0.26964	0.27392
3.0	0.27780	0.28132	0.28451	0.28742	0.29008	0.29252	0.29475	0.29681	0.29871	0.30046
4.0	0.30208	0.30359	0.30499	0.30629	0.30751	0.30864	0.30970	0.31070	0.31163	0.31251
5.0	0.31333	0.31411	0.31484	0.31553	0.31619	0.31680	0.31739	0.31794	0.31847	0.31897
6.0	0.31944	0.31990	0.32033	0.32074	0.32113	0.32150	0.32185	0.32219	0.32252	0.32283
7.0	0.32313	0.32341	0.32369	0.32395	0.32420	0.32444	0.32468	0.32490	0.32512	0.32532
8.0	0.32552	0.32571	0.32590	0.32608	0.32625	0.32641	0.32657	0.32673	0.32688	0.32702
9.0	0.32716	0.32730	0.32743	0.32755	0.32767	0.32779	0.32791	0.32802	0.32813	0.32823

Derivative of F(E)

A	0.0	0.1	0.2	0.3	0.4	0.5	0.6	0.7	0.8	0.9
0.0	0.0	0.01774	0.03528	0.05240	0.06888	0.08447	0.09890	0.11192	0.12323	0.13260
1.0	0.13979	0.14465	0.14711	0.14718	0.14500	0.14079	0.13485	0.12757	0.11934	0.11054
2.0	0.10153	0.09262	0.08403	0.07595	0.06847	0.06165	0.05549	0.04998	0.04508	0.04074
3.0	0.03689	0.03349	0.03048	0.02780	0.02543	0.02332	0.02143	0.01974	0.01822	0.01686
4.0	0.01562	0.01451	0.01350	0.01258	0.01174	0.01097	0.01027	0.00963	0.00904	0.00850
5.0	0.00800	0.00754	0.00711	0.00672	0.00635	0.00601	0.00569	0.00540	0.00513	0.00487
6.0	0.00463	0.00441	0.00420	0.00400	0.00381	0.00364	0.00348	0.00332	0.00318	0.00304
7.0	0.00292	0.00279	0.00268	0.00257	0.00247	0.00237	0.00228	0.00219	0.00211	0.00203
8.0	0.00195	0.00188	0.00181	0.00175	0.00169	0.00163	0.00157	0.00152	0.00147	0.00142
9.0	0.00137	0.00133	0.00128	0.00124	0.00120	0.00117	0.00113	0.00110	0.00106	0.00103

If the particles are assumed to be cylindrical in shape,

and $\alpha \cong \frac{(A')^2 V}{\ln A'}$ where $(A') = \frac{\text{length}}{\text{diameter}} = \frac{\ell}{d}$ and

V = Volume = $\pi(\frac{d}{2})^2 \ell$

then $\alpha \cong \frac{\pi \ell^3}{4 \ln(\frac{\ell}{d})}$ (16)

If a set of particle dimensions are assumed a plot of f(E) vs A where $A = \frac{\alpha E^2}{2kT}$ will show the general shape of the response, f(E), as the E-field strength is increased. Figure 8 shows the predicted general line shape.

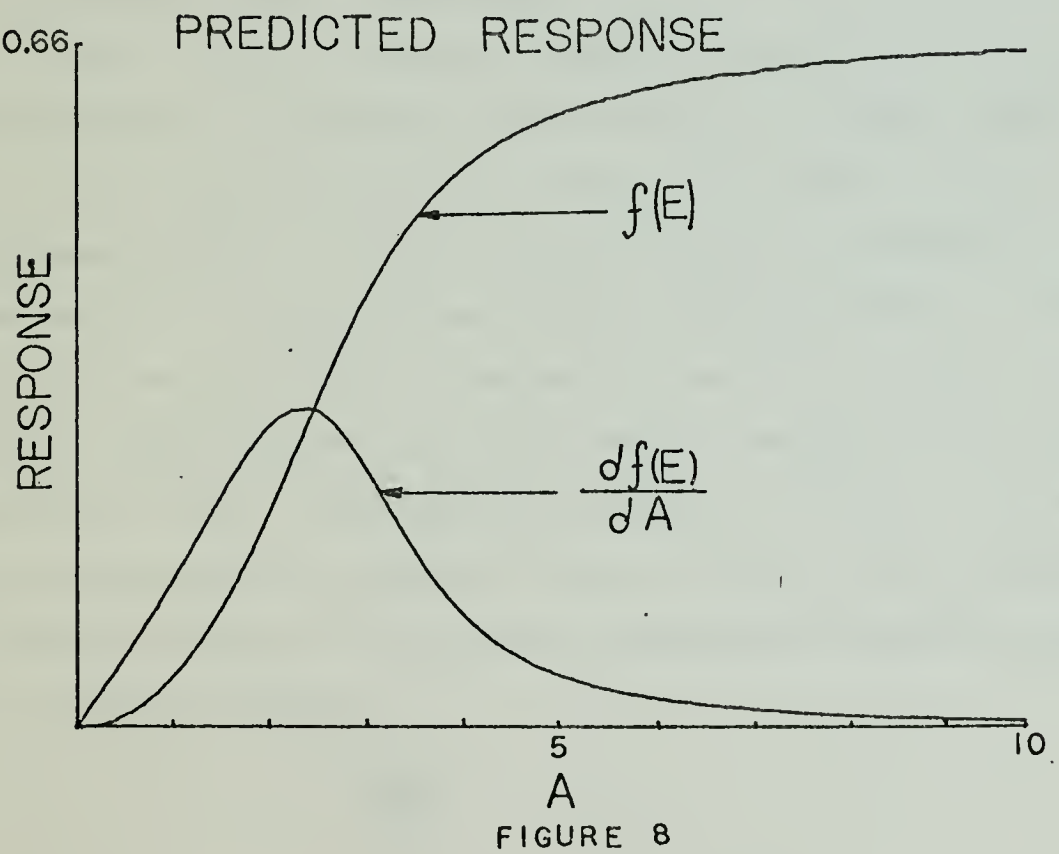

FIGURE 8

It is shown that the response is not a linear function of the applied E-field and will saturate. This curve, it should be noted, is for only one size particle, one value of α. If a distribution of different size particles, which implies a spread in α values, is present the overall response will be an average of these different line shapes which has the effect of flattening the curve and making the maximum slope lower.

Values of $\frac{df(E)}{dA}$ are also given in Figure 8. For this graph as stated previously, a distribution in particle size will also tend to distort the predicted curve shape, causing a general flattening of the peak response.

C. RELAXATION TIME (FREQUENCY)

Debye in Ref. 1 defines relaxation time as "the time required for the moments of the molecules to revert practically to a random distribution after the removal of the impressed field." If the impressed field is modulated at a frequency, ν, corresponding to this relaxation time, τ, the particle response will be degraded because the moments can not be induced in the particles rapidly enough to follow the modulated field. Carrington and McLachlan in Ref. 14 give the characteristic relaxation time in terms of the viscosity, μ, and the radius, a, of a sphere undergoing Brownian motion in a viscous fluid as:

$$\tau = \frac{4\pi\mu a^3}{3kT} \quad .$$

This expression was derived from the Debye equation and the viscous torque, T, on a spherical object where

$$T = 8\pi\mu a^3\omega$$

and ω = angular velocity of the sphere.

Happel and Brenner in Ref. 15 extended the treatment to non-spherical particles by expanding the viscous torque in a series of spherical harmonics. This development showed that for particles having only small deviations from a sphere, eccentricities of approximately 0.8, the relaxation phenomena followed that predicted for a sphere with a volume equal to the volume of the ellipse. For higher eccentricities, necessary to approximate a cylinder, higher order spherical harmonic terms would have to be evaluated. To avoid this necessity, another approach would be to investigate the drag on a cylinder translating through a viscous medium in a direction perpendicular to its axis of symmetry. Lamb in Ref. 16 gives the resistance for a cylinder per unit length as

$$dT = \frac{4\pi\mu\ U\ d\ell}{\frac{1}{2} - \gamma - \ln(\frac{r\omega\ell}{4\xi})}$$

where r is the radius of the cylinder, γ = Euler's constant = 0.5772156649 from Ref. 17, ξ = kinematic viscosity = μ/ρ, $U = \omega\ell$, and ρ = density.

Then

$$dT = \frac{4\pi\mu U \ell d\ell}{\frac{1}{2} - \gamma - \ln(\frac{r\omega\ell}{4\xi})} = \frac{4\pi\mu\omega\ell^2 d\ell}{\frac{1}{2} - \gamma - \ln(\frac{r\omega\ell}{4\xi})}$$

if $\omega = \sqrt{\frac{kT}{I}}$ and $I = \frac{ML^2}{12} = \frac{\pi r^2 L^3 \rho}{12}$

for a rod where L = length of the cylinder, then

$$\omega = \sqrt{\frac{12kT}{\pi r^2 L^3 \rho}} \quad .$$

Now define the dimensionless parameter, x

$$x \equiv \frac{2\ell}{L} \quad ; \quad \text{at} \quad \ell=0,\ x=0,\ \ell=\frac{L}{2},\ x=1$$

upon substitution

$$dT = \frac{4\pi\mu\omega(\frac{L}{2})^3\, x^2 dx}{\frac{1}{2} - \gamma - \ln K^{1/2} x}$$

where

$$K = \frac{3kT}{16\pi\ \xi^2\ L\ \rho} = \frac{3kT\rho}{16\pi\ \mu^2\ L}$$

then:

$$T = 8\pi\mu\omega\left(\frac{L}{2}\right)^3 \int_0^1 \frac{x^2\,dx}{1 - 2\gamma - \ln K - 2\ln x} \qquad (17)$$

Under Lamb's development for dT, K was required to be $<< 1$, therefore $-\ln K$ will dominate the denominator as $x \to 1$. $-2(\ln x)$ can be neglected because as $x \to 1$, $-2(\ln x) \to 0$; however, this term has a large value, $\to -\infty$, as $x \to 0$ but in this region, small x, the value of the integral is very small and to a first approximation the integral is:

$$\int_0^1 \frac{x^2\,dx}{1 - 2\gamma - \ln K - 2\ln x} \cong \int_0^1 \frac{x^2\,dx}{1 - 2\gamma - \ln K} = \frac{1}{3(1 - 2\gamma - \ln K)}$$

therefore

$$T = 8\pi\mu\omega\left(\frac{L}{2}\right)^3 \left[\frac{1}{3(1 - 2\gamma - \ln K)}\right] . \qquad (18)$$

Let

$$S = \frac{1}{3(1 - 2\gamma - \ln K)} .$$

It should be noted that this equation gives the cylinder's viscous torque in terms of the viscous torque for an equivalent sphere whose radius is 1/2 the length of the cylinder multiplied by a correction term, S, for the geometry and type of particle.

From Einstein's relation

$$\tau = \frac{T}{6kT\omega}$$

therefore

$$\tau_c = \frac{8\pi\mu(\frac{L}{2})^3}{6kT} S$$ = relaxation time for a given

cylindrical rod and the relaxation frequency is

$$\nu_{relax} = \frac{1}{2\pi\ \tau_c} \qquad (19)$$

If one assumes that the particles effectively respond as a cylinder and that these cylinders are translating in a viscous medium of air, then predicted relaxation times and frequencies can be determined for a range of particle sizes. Predicted values for K, S, τ_c, and ν(relax) are given in Table III for ZnO particles ranging from 1 to 4 microns length. The temperature was assumed to be 300°K, $\mu \cong 183$ μpoise is the viscosity of air at 300°K and $\rho = 5.6$ gm/cm^3 as the density of ZnO.

D. PARTICLE SIZE DISTRIBUTION

Starting with the general equation for motion as a description of the response of the particles, the amplitude of the response will vary as

$$\frac{1}{1 - i\tau_c\omega} \qquad (20)$$

PARTICLE SIZE (cm)	K	S	τ_c (sec)	ν_{relax} (Hz)
1.0×10^{-4}	4.13×10^{-3}	5.64×10^{-2}	1.31×10^{-4}	1219
1.5×10^{-4}	2.75×10^{-3}	5.28×10^{-2}	4.12×10^{-4}	386
2.0×10^{-4}	2.07×10^{-3}	5.05×10^{-2}	9.35×10^{-4}	170
2.5×10^{-4}	1.65×10^{-3}	4.88×10^{-2}	1.76×10^{-3}	90
3.0×10^{-4}	1.38×10^{-3}	4.76×10^{-2}	2.97×10^{-3}	53
3.5×10^{-4}	1.18×10^{-3}	4.65×10^{-2}	4.61×10^{-3}	34
4.0×10^{-4}	1.03×10^{-3}	4.57×10^{-2}	6.77×10^{-3}	24

Predicted Relaxation Frequencies and Times

for ZnO Cylinders

TABLE III

The general form for the real and imaginary components of this function for a single value of τ as a function of ω is given by figure 9.

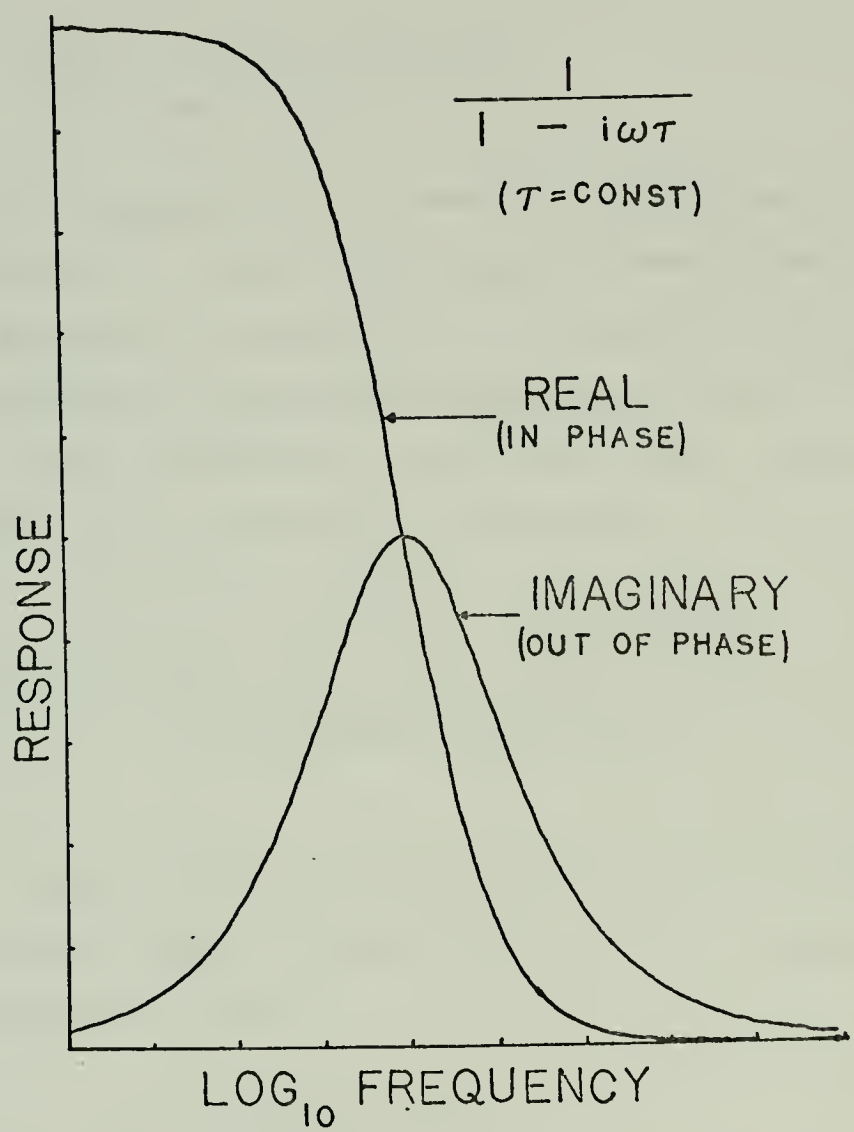

FIGURE 9

However in reality there exists a distribution of particle sizes and consequently a distribution in τ_c's. To include the effects due to the distribution in τ_c's, values for the shape of equation 20 must be averaged over all τ_c values.

If there exists a function of two parameters ω and τ, $f(\omega,\tau)$, and there is a distribution in the values for τ, then the observed function will be a function of ω averaged over the τ values:

$$R(\omega) = \int_{-\infty}^{\infty} f(\omega,\tau)\, P(\tau)\, d\tau$$

$P(\tau)$ = probability distribution function and is the probability that $f(\omega,\tau)$ has a value between τ and $\tau + d\tau$.

A log-normal distribution is frequently found for functions where negative τ's are not physically realized, but where small values must be included in the distribution. Using this function as the probability distribution:

$$R(\omega) = \frac{\int_{0}^{\infty} f(\omega,\tau)\, \exp\{-\sigma(\ln \tau/\tau_o)^2\}\, d(\ln \tau)}{\int_{0}^{\infty} \exp\{-\sigma(\ln \tau/\tau_o)^2\}\, d(\ln \tau)} \qquad (21)$$

where σ is a measure of the spread in τ's. By defining $x \equiv \ln \tau/\tau_o$ then $dx = d(\ln \tau)$, $\tau = \tau_o e^x$ and substituting in equation (21) then

$$R(\omega) = \frac{\int_{-\infty}^{\infty} f(\omega,\tau_o e^x)\, e^{-\sigma x^2}\, dx}{\int_{-\infty}^{\infty} e^{-\sigma x^2}\, dx}$$

or

$$R(\omega) = \sqrt{\frac{\sigma}{\pi}} \int_{-\infty}^{\infty} f(\omega, \tau_o e^x)\ e^{-\sigma x^2}\ dx$$

The spread in τ's is given roughly as: $\sigma(\ln \tau/\tau_o)^2 = 1$,

$\ln \tau/\tau_o = 1/\sqrt{\sigma}$ thus $\Delta(\ln \tau/\tau_o) \cong 2/\sqrt{\sigma}$

If $\tau_o = 1$

$$R(\omega) = \sqrt{\frac{\sigma}{\pi}} \int_{-\infty}^{\infty} \frac{1}{1 - i\omega e^x}\ e^{-\sigma x^2}\ dx \qquad (21a)$$

or as σ increases, the spread in τ's decrease. Using the function $\frac{1}{1 - i\omega\tau}$, figure 10 depicts the shape of the function for various values of σ.

By taking the ratio of the magnitude of the peak imaginary response to the real response, a measure of σ can be obtained. From this the spread in τ's can be inferred which then leads to the distribution in particle sizes.

A table of this ratio as a function of σ is given by Table IV. This table was obtained by numerical integration on a Hewlett Packard Model 9810 calculator.

σ	RATIO	σ	RATIO
10.0000	0.4882	0.2512	0.3144
7.9433	0.4854	0.1995	0.2944
6.3096	0.4819	0.1585	0.2742
5.0119	0.4777	0.1259	0.2541
3.9811	0.4726	0.1000	0.2343
3.1623	0.4665	0.0794	0.2151
2.5119	0.4593	0.0631	0.1966
1.9953	0.4509	0.0501	0.1791
1.5849	0.4411	0.0398	0.1626
1.2589	0.4299	0.0316	0.1471
1.0000	0.4173	0.0251	0.1328
0.7943	0.4031	0.0200	0.1195
0.6310	0.3876	0.0159	0.1073
0.5012	0.3708	0.0126	0.0960
0.3981	0.3529	0.0100	0.0857
0.3162	0.3340	0.0079	0.0762

Calculated Ratio of Peak Imaginary/Peak Real Response for a Given Value of σ

TABLE IV

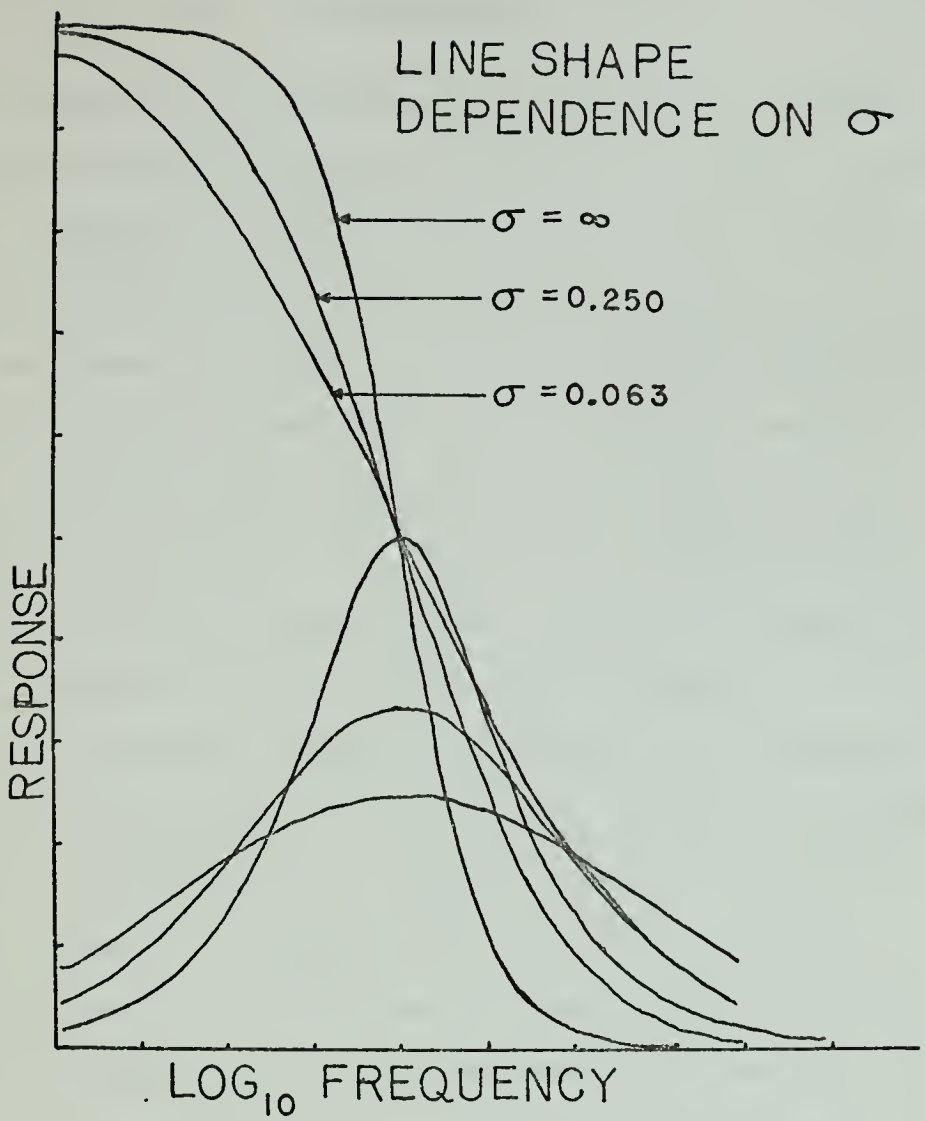
LINE SHAPE
DEPENDENCE ON σ
σ = ∞
σ = 0.250
σ = 0.063
RESPONSE
LOG10 FREQUENCY

FIGURE 10

III. EXPERIMENTAL

In the design of an experimental apparatus to observe and record the expected dielectric response, certain requirements were considered essential and methods were developed to meet these requirements. The first requirement to be met was the development of a method for the continuous production of a dielectric particulate suspension so that a continuous flow could be introduced into a microwave cavity where the effect would be produced. The next step in the evolution of the effect was the design and construction of microwave cavities which allowed the particles to be introduced and expelled and an external voltage potential applied so that preferential particle alignment could take place. The final requirement was the development of a system of supporting and recording equipment to supply the microwave energy and desired frequencies, the external voltage modulation, and a means of detecting the modulated response from the cavity and recording the response. To this end the following sections on SAMPLE PREPARATION AND PARTICULATE SUSPENSION PRODUCTION, CAVITY DESIGNS, AND EXPERIMENTAL APPARATUS explain the evolution leading to a method for the characterization of the dielectric response.

A. SAMPLE PREPARATION AND PARTICULATE SUSPENSION PRODUCTION

Two different compositions of tubular sample cores were utilized to produce zinc oxide particles in the vapor phase.

One core was reagent grade zinc oxide (ZnO) and the other was a ZnO core doped with a 0.05 mole % indium (In). The preparation of the ZnO core was accomplished by compressing 150 to 200 grams of reagent grade ZnO powder in a coaxial cylinder forming a thick tube of the packed powder. This tube was then placed in a furnace and sintered at 900° C for approximately 4 $\frac{1}{2}$ hours, producing a very hard, brittle core of ZnO.

In order to produce the desired indium doped sample, it was necessary to produce indium sesquioxide (In_2O_3) which is a yellowish orange powder and can be readily mixed with ZnO powder. This oxide was produced by heating a quantity of 99.99 % pure indium wire in a combustion boat in a mullite tube placed through a LINDBERG/HEAVIDUTY furnace at 1150° C for approximately 1 $\frac{1}{2}$ hours. Complete oxidation of the indium was insured by scraping and crushing the partially oxidized mixture after it had been heated for approximately 35 minutes and forcing a flow of air across the boat by means of the draft effect set up by an exhaust hood surrounding one end of the mullite tube.

Once the In_2O_3 was prepared, the oxide was finely crushed and thoroughly mixed with sufficient ZnO to produce a doping concentration of 0.05 mole % In in ZnO. This mixture was then sintered in exactly the same way as the reagent grade ZnO cores were sintered. Suspended ZnO particles were produced from these cores by first reducing the solid ZnO with hydrogen gas, releasing metallic zinc vapor, and oxidizing

the metallic zinc with oxygen producing a dispersed suspension of ZnO particles. Figure 11 is a cutaway view of the furnace tube arrangement used for particulate suspension production. The method of production was similar to that employed by Dodson and Savage in Ref. 18 to produce single crystal ZnO. This production was carried out in a mullite tube configured LINDBERG/HEAVIDUTY furnace at temperatures between 1300° C and 1000° C. Figure 27 shows the size particle produced vs temperature of production. Hydrogen was introduced into the tube using nitrogen as a carrier gas. It was necessary to use nitrogen as a carrier because the low hydrogen flow rates would not have been sufficient to create the necessary positive down-tube flow of gas and metallic zinc. The tubular design of the zinc oxide core allowed a second quartz glass tube to be passed through the core's center to introduce the oxygen gas after the reduction of the ZnO core had taken place. Both ends of the tube were stoppered with asbestos wrapped teflon stoppers drilled to accommodate the gas tube. The hot gases and suspended ZnO particles were then expelled from the furnace and introduced, via a glass (pyrex) tube, into the microwave cavity being used. It was assumed that the gas and particles had cooled to room temperature (300° C) by the time of introduction into the cavity. Figures 12(a) and 12(b) are pictures of scanning electron microscope (SEM) images of the ZnO particles produced in the above manner.

For experiments utilizing the reflection apparatus a tubular furnace capable of only 1100° C temperatures was

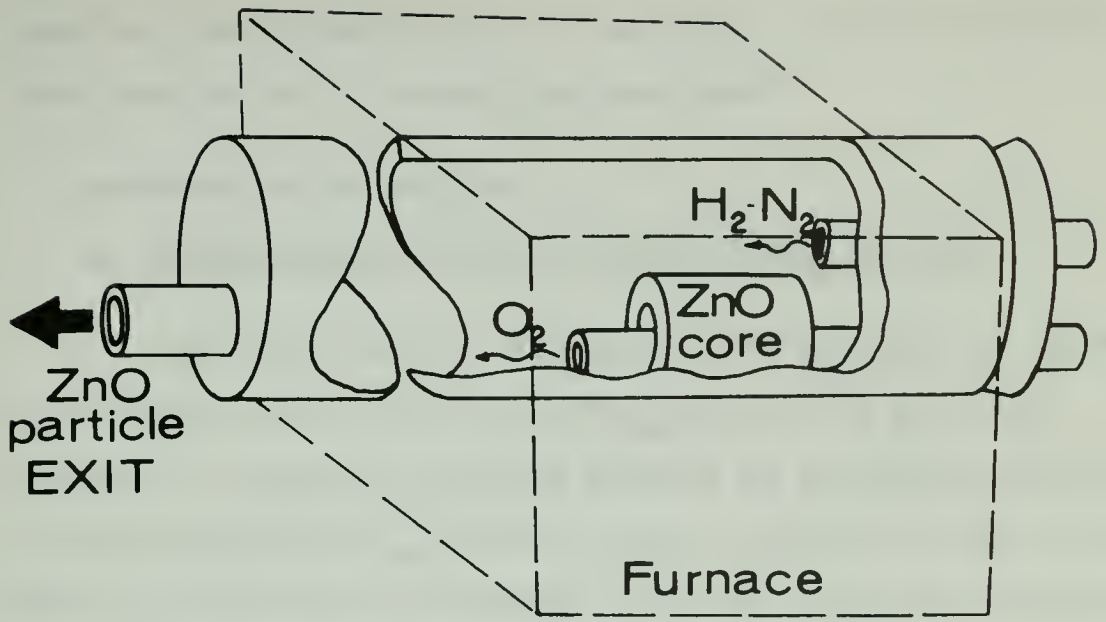

Figure 11

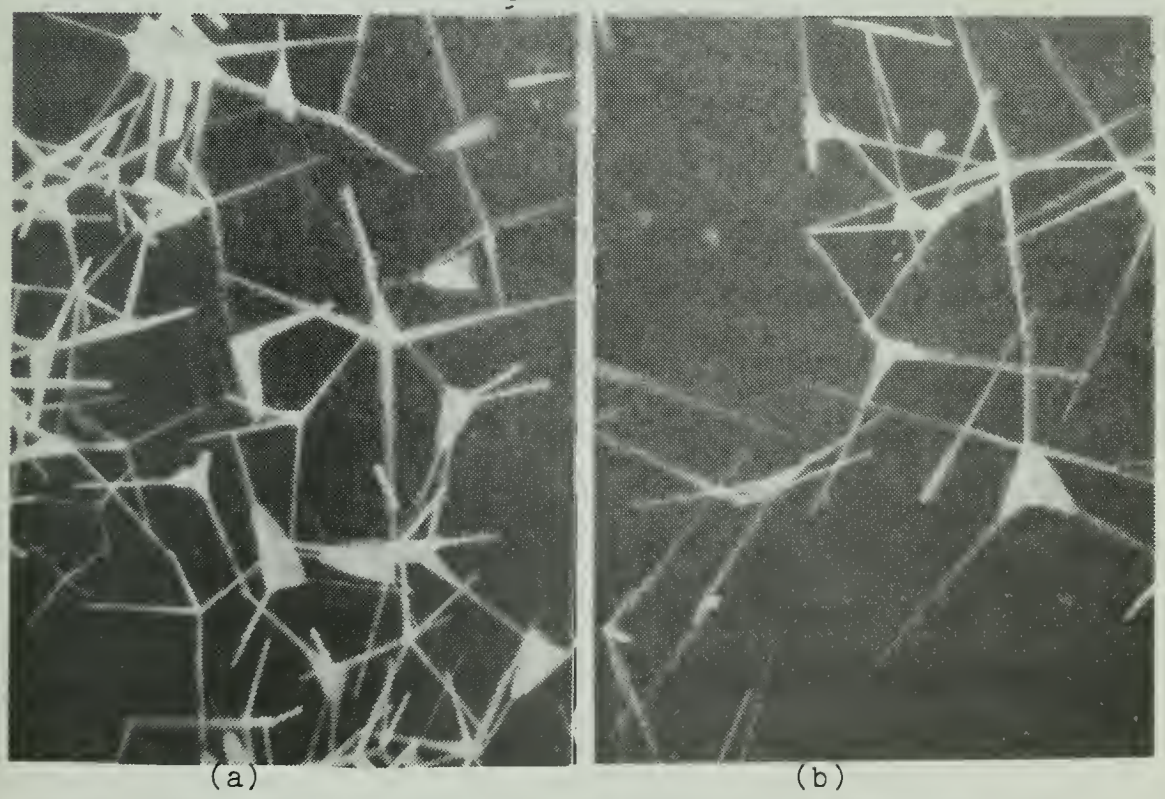

(a) ZnO Particles Produced at 1200°C 1μ

(b) ZnO Particles Produced at 1250°C 1μ

Figure 12

used for the production of ZnO particles. The same type cores and method of production were used.

B. RESONANT CAVITY DESIGNS

1. Rectangular - Flat Plate Reflection Cavity

The first cavity, figure 13, was designed to operate as a reflection cavity in the TE_{102} mode. It was also designed to allow an external E-field to be impressed parallel to the microwave TE_{102} E-field lines, figure 13, and to allow ZnO particles to be introduced into the cavity so that changes in the microwave resonance could be observed. The rectangular cavity was made from standard (0.4" X 0.9") X-band waveguide material cut to a 5 cm length so that the cavity would resonate in the TE_{102} mode at 8.88 GHz. 8.88 GHz was chosen because it corresponded to the approximate peak of a mode of the V-153C klystron used in the X-band microwave bridge associated with the Varian unit. Standard waveguide flanges were added to each end and a quick connect/disconnect clamp was added to the input end to facilitate the connection/disconnection of the cavity to/from the transmission waveguide. This feature was incorporated because it was necessary to remove the cavity from time to time to clean out precipitated particles. A 0.25" diameter circular iris coupling port was used to couple the microwave energy into the cavity from the waveguide.

Particle entry and exit ports were constructed at the geometric center of the cavity length on the narrow

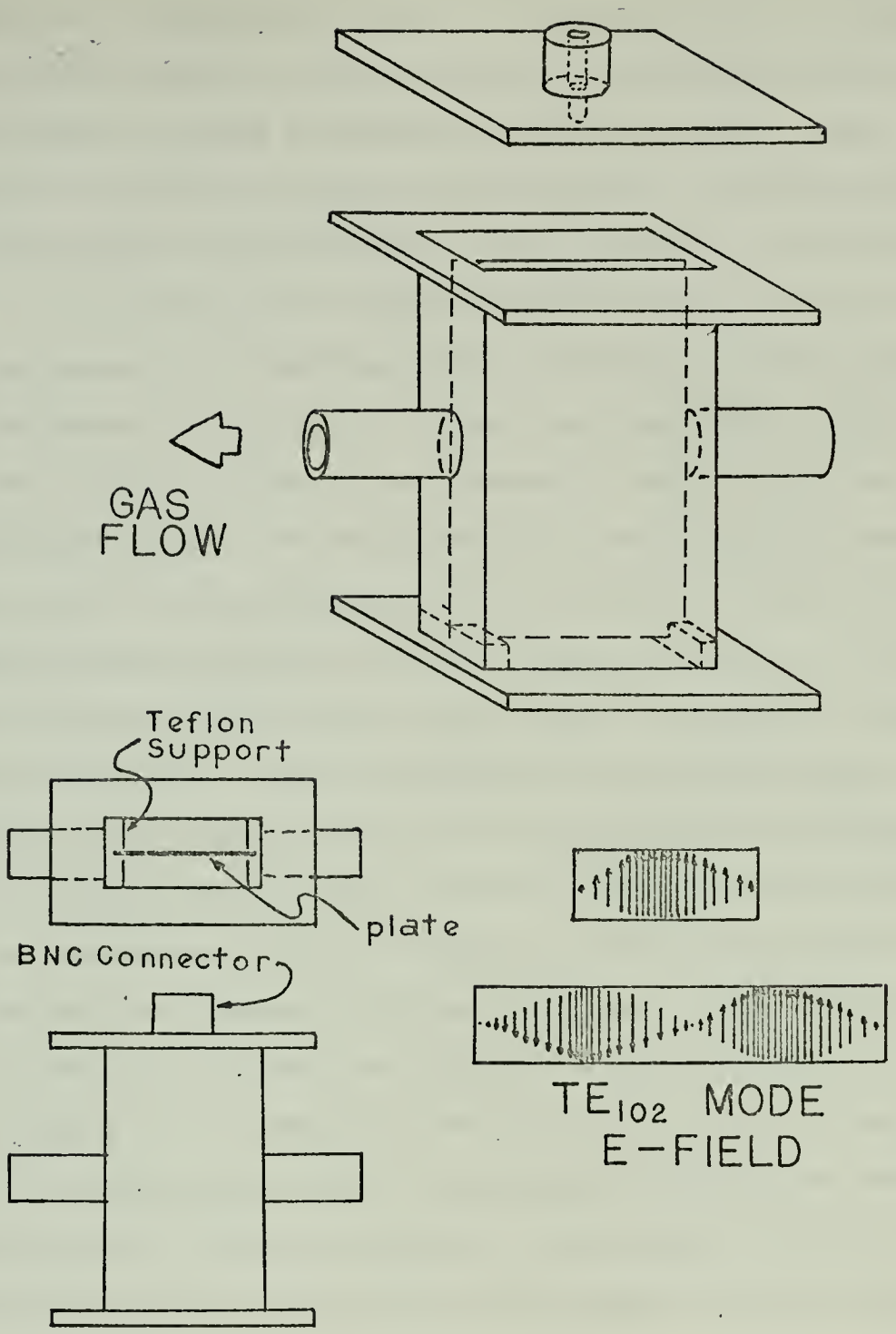

RECTANGULAR REFLECTION CAVITY

FIGURE 13

dimension. Sleeves were added to trap any microwave energy which might penetrate the entry/exit holes and otherwise be lost thereby causing a lowering of cavity quality. The geometric center was chosen because the TE_{102} E-field pattern is a minimum at this wall, and a node exists at the center.

A 0.010" brass plate was inserted half way down the narrow dimension, extending across the width and down the entire length of the cavity. The plate was held in place by four slotted teflon pieces located in each corner, and was insulated from the cavity walls by air spacing of approximately 1/16". This arrangement of the plate to the cavity dimensions was chosen so that an external E-field when applied across the plate and cavity walls would be parallel to the microwave E-field. This arrangement also presented the smallest resistance to the flow of the incoming gas particles. Also by isolating the plate from the walls, the plate does not act as a microwave guiding boundry. Teflon was chosen because of its low loss characteristics and placed in the corners where the field patterns are minimal. A BNC type connector was mounted in the far end plate away from the iris coupling port. A pinch-type connector was fashioned from the center conductor of the BNC and attached to the plate. The BNC connector was then connected to the external voltage source for application of the external field.

The reflection cavity was abandoned due to the limitations imposed by the fixed iris coupling and the Varian unit as explained in Section IVA. Even though the reflection

cavity was unsatisfactory, many of the parts and concepts were carried over to the rectangular transmission cavity.

2. Rectangular - Flat Plate Transmission Cavity

The second cavity design, figure 14, incorporated the same geometry of external field to microwave fields as in the reflection cavity. The main differences were in the method of coupling the microwave energy into the cavity and the frequency of the cavity resonance. This cavity operated as a transmission cavity whereas the previous design was a reflection cavity. A cavity length of 6 cm provided a resonance at 8.4 GHz. Microwave coaxial probe coupling was utilized to excite the cavity in the TE_{102} mode. Ports for the coupling probes were placed 1.5 cm from one end opposite each other centered on the wide cross-sectional dimension. This position was chosen because the field pattern for the TE_{102} mode has a maximum at this point and provides the most efficient coupling. Brass sleeves were added to the ports to insure that the probe would remain at the position needed to provide proper coupling and prevent microwave leakage from the cavity. Particle entry and exit, the BNC method for voltage application, and flat plate were identical to the methods already described for the reflection cavity.

The attempts to classify the response from the above resonant cavity proved inconclusive. The reasons for this conclusion are given in Section IVA. Because of these difficulties, the rectangular cavity was abandoned.

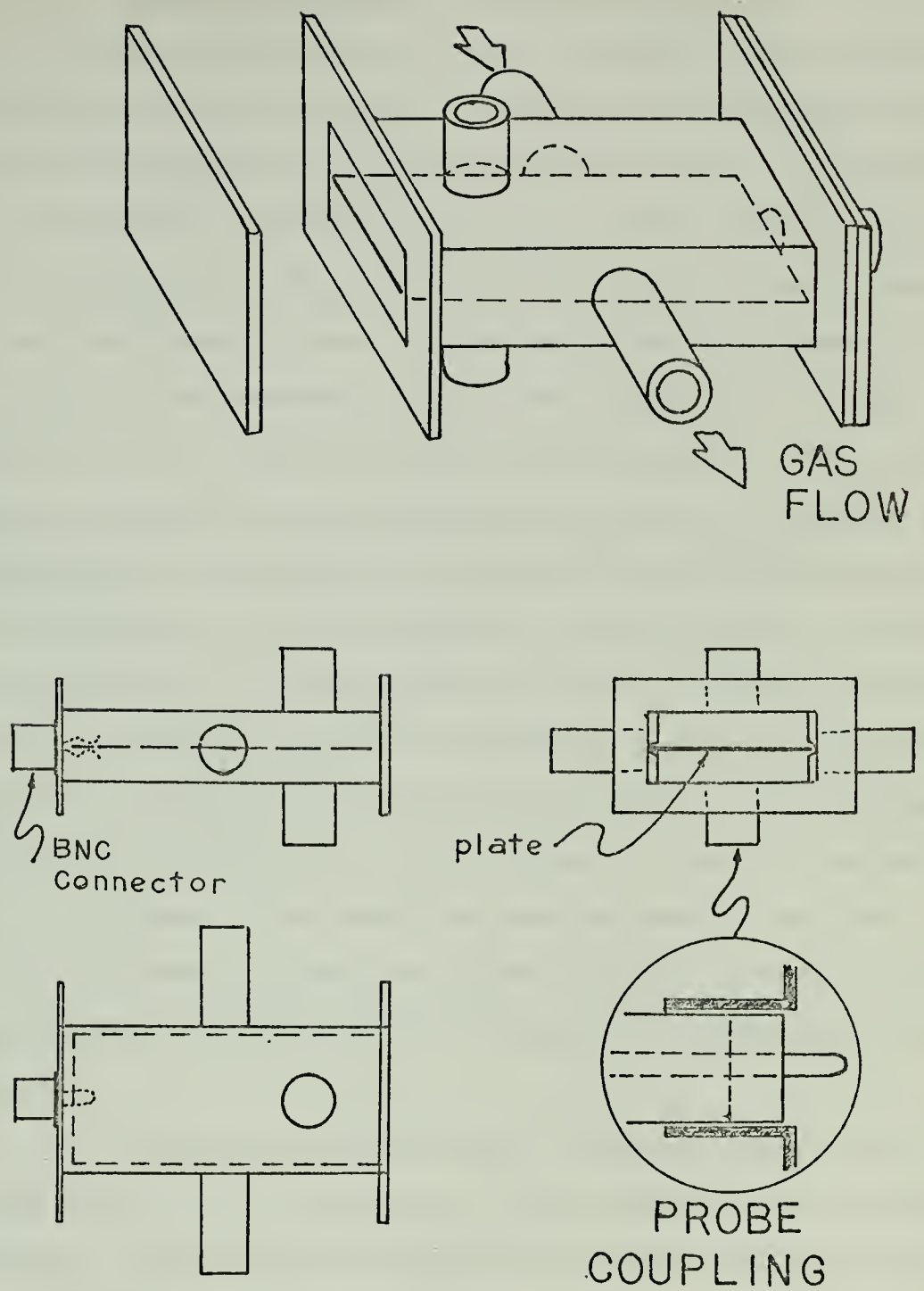

RECTANGULAR TRANSMISSION CAVITY

FIGURE 14

3. Cylindrical Coaxial Transmission Cavity

The third and final cavity, figure 15, was designed so that the applied external E-field would be perpendicular to the microwave standing wave E-field pattern. A cylindrical cavity with a solid brass inner rod was utilized because the coaxial cavity TE_{012} mode has an E-field which is parallel to and diminishes to zero at the cavity walls, figure 15. By applying the external E-field from inner rod to outer cavity wall the desired geometry was obtained. The externally applied E-field is not homogeneous and shows a 1/radius type dependence. To diminish the effect of the 1/radius variation in the external E-field strength, it was desirable to construct the cavity from a large diameter circular cylinder with the inner rod having as large a diameter as possible and still support resonance at the desired frequency. A 5.4 cm brass cylinder was used with a 2.4 cm brass rod located concentric to the cylinder. The inner rod was designed to be $\frac{1}{2}$ cm shorter on each end than the outer cylinder allowing a centrally located particle entry and exit port and free particle flow.

Particles were introduced into the cavity from a central port on the front face of the cavity. Exit was provided by a port at the far end of the cavity centrally located in the end plate. Microwaves were introduced via coaxial transmission lines to magnetic loop type coupling from ports located at opposite ends of a diameter approximately 1 cm from the forward end plate. "Scotch" brand transparent tape

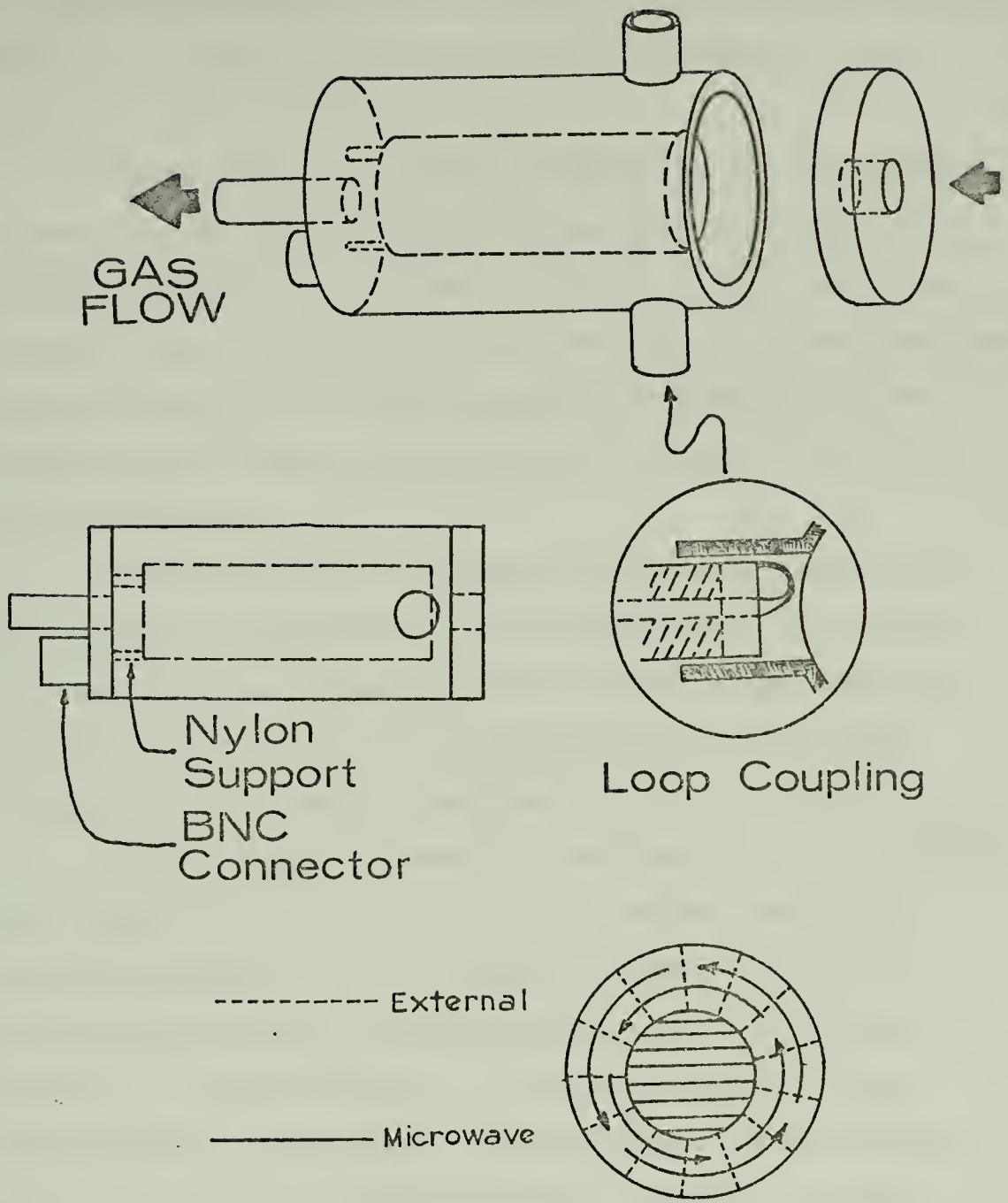

Electric Field Configuration

CYLINDRICAL COAXIAL CAVITY

Figure 15

was placed over these ports to prevent particles from accumulating in the ports and affecting the efficiency of the coupling.

Nylon screws were threaded from the rear plate into the inner rod and held firmly by means of nylon nuts also serving as spacers. A hole was drilled in one nylon screw to allow a wire to be connected to the inner rod and insulated from the outer wall. A BNC connector was inserted in the rear plate as a means of introducing a potential from inner rod to outer wall.

As noted in the rectangular cavity, the cavity had to be cleaned periodically. To facilitate this the cavity front end plate was connected with a single screw allowing the plate to be swung open and vacuumed out with minimum disturbance to the cavity coupling.

Even though the inner rod was designed to be approximately one cm shorter than the cavity length, the entire cavity was assumed to be a coaxial cylinder. Under this assumption and using the development as given by Beringer, equation 2, a cavity length of 6 cm will produce a TE_{012} resonant mode at 11.34 GHz. Five relatively closely spaced modes were present when the microwave frequency was swept from 8 to 12 GHz. A strong mode assumed to be the TE_{012} mode was present at 11.35 GHz and was utilized as the resonant frequency for follow on experiments. It was assumed that the shorter inner rod had the effect of removing the degeneracy caused by the TM_{112} mode.

C. EXPERIMENTAL APPARATUS

1. Reflection Cavity Equipment

a. Microwave Resonant Cavity

The rectangular-flat plate reflection cavity as described in Section IIIB1 was utilized with this apparatus. The cavity was mounted vertically allowing good particle and effluent entry/exit and easy access to the quick connect/disconnect clamp so that the cavity could be easily cleaned. Figure 16 shows the arrangement of the cavity in the apparatus.

b. Varian Unit

The Varian Unit was configured with the model V4500-10A EPR Control Unit, model V4595 Selector Panel and a Hewlett-Packard HP-120B Oscilloscope. The V4500-10A unit functioned as a lock-in amplifier, phase sensitive detector, and a sine wave modulation source. The lock-in amplifier function was necessary to detect and amplify modulation frequencies of 20, 40, 100, 200, and 400 Hz. The phase sensitive detector was necessary to detect the in-phase-with-reference signal. It also functioned as the power source for the V-153C klystron utilized in the Microwave X-band bridge. A Hewlett-Packard model HP X-532B Frequency Meter (wave meter) was utilized to obtain the approximate cavity resonance frequency and provided a means to calibrate the HP120B Oscilloscope so that approximate cavity Q could be determined. It was determined that the reflection cavity Q was on the order of 1100.

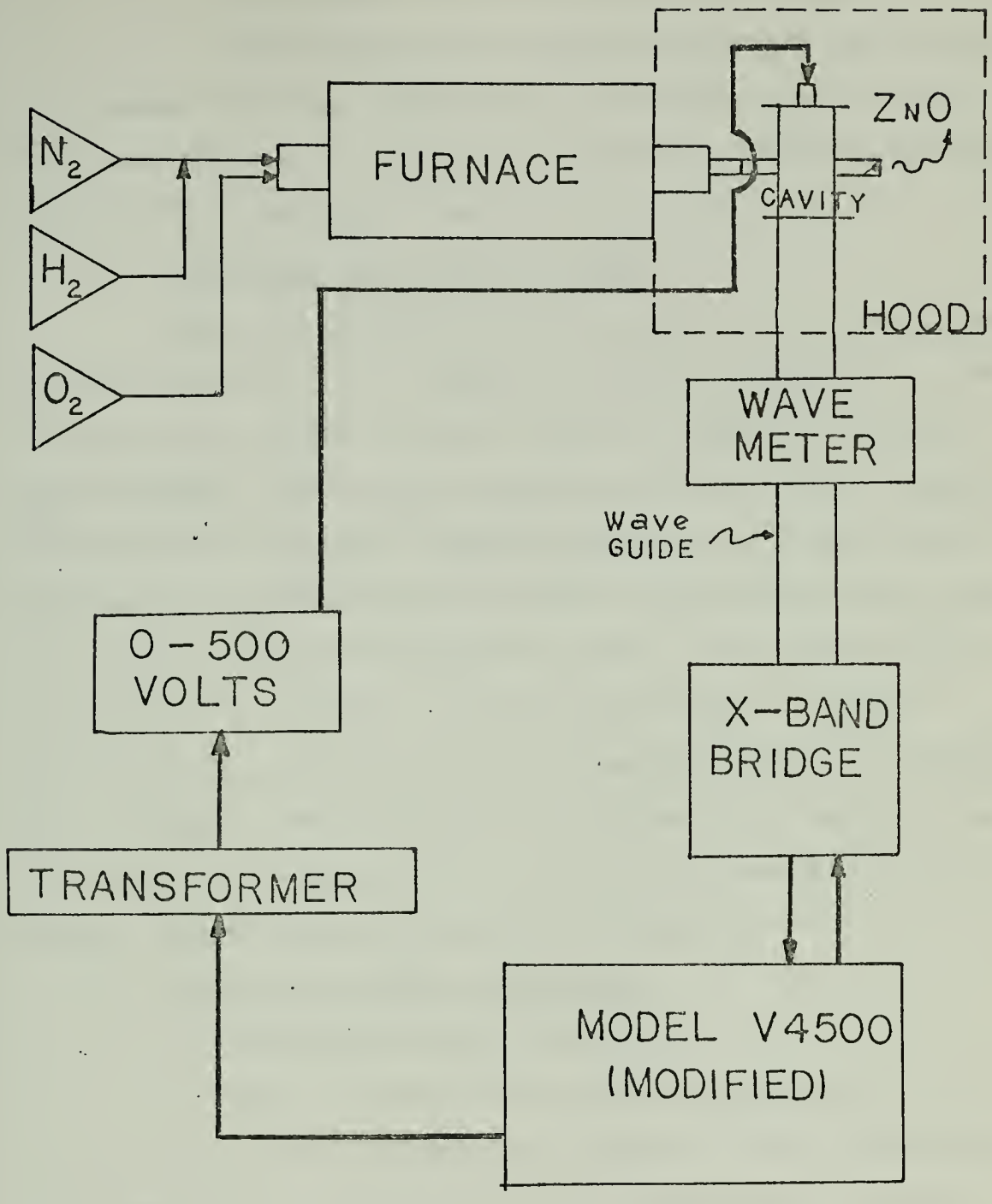

REFLECTION CAVITY APPARATUS

FIGURE 16

c. Transformer And 0-500 Volt Power Supply

The transformer (turns ratio 50:110) was utilized to increase the sine wave modulation V4500-10A output amplitude peak to peak to 100 volts and the 0-500 volt power supply suuplied a DC biasing to the sine modulation.

2. Reflection Cavity Block Diagram

Figure 16 provides a block diagram of the reflection cavity apparatus. A 2" diameter hole was drilled into a wall of the hood to allow the tube from the furnace to protrude into the hood. The tube, containing the ZnO core as explained under Section IIA, was tightly plugged at each end so that the gases were forced down the tube, over the ZnO core, into the glass tube, and through the cavity. Some system leaks were present; however, the leaks were only slight and expulsion of particles from the tube and through the cavity was obtained. The exhausted ZnO particulate suspension was removed by the exhaust hood, removing the possibility of a health hazard from inhalation of the smoke.

3. Transmission Cavity Equipment

a. Microwave Resonant Cavities

The rectangular-flat plate transmission and the cylindrical coaxial transmission cavities were utilized with this apparatus. These cavities were described in Section IIIB2 & IIIB3. The sample, ZnO, was introduced into the cavity by a glass tube from the furnace tube end to the cavity particle entry port. The glass tube was constructed with a flexible rubber joint to allow access to the cavity for cleaning

without having to disturb sample production or microwave coupling into the cavity. Since the cavities were transmission type, crystal detectors were used to detect the microwave energy and transmitted via coaxial cables to the Princeton Applied Research (PAR) lock-in amplifier/phase detector. The crystals used were Hewlett Packard model HP423A or model HP8470A crystal detectors.

b. Hewlett-Packard HP 8690B Sweep Oscillator

The sweep oscillator operated in the 8-12 GHz region to supply the resonant cavity microwave fields. The output frequency was swept at various rates across a band of frequencies sufficiently wide to observe a resonant cavity mode. The variable sweep speed was utilized to allow sufficient modulation time for a detectable response across the resonant mode. A 20 dB Hewlett-Packard model HP779D directional coupler was connected to the oscillator output to sample the output and send a small signal through a Beckman/Berkeley Transfer Oscillator model 7580 to an R-390/URR Radio Receiver (500 KHz to 32 MHz). The output from the R-390 was used as the negative vertical input to a Tektronix Type 503 Oscilloscope to provide 5 MHz calibration spikes on the scope face.

These calibration spikes provided a means for determining the sensitivity of the cavity, or cavity Q, and how much effect the internal plate, for the rectangular cavity, or the inner rod, for the cylindrical cavity, had on the cavity Q. The Q was measured as the resonant frequency divided

by the width of the resonance at half maximum (3 dB point) on the scope. Q determinations were made before and after modifications from the basic rectangular and cylindrical cavity. The rectangular cavity Q was lowered from approximately 4800 to 2900 and the circular cavity from approximately 5000 to 3000.

c. Princeton Applied Research Lock In Amplifier/Phase Detector, Model 121

The lock-in amplifier was required to lock onto a given modulation frequency, supplied as reference to the amplifier, and detect the presence of this frequency signal in the signal transmitted from the resonant cavity. Phase detection was necessary to discriminate between the transmitted real (in phase with reference) and imaginary (90° out of phase with the reference) response in order to obtain the peak real to imaginary ratio for determination of particle size distributions.

The alignment and proper phasing of the model 121 was accomplished by taking the output from the Square Wave Generator and utilizing this output as both reference and input response. The input was first attenuated by a fixed 100K attenuator to approximate the power levels expected from the resonant cavity. The reference level was always fixed at half of the maximum scale reading, then the lock-in frequency was adjusted to match the output from the Square Wave Generator by turning the frequency control knob until a maximum deflection was obtained on the scale.

To insure that the phase detector was properly aligned the phase function switch was changed from 0° phase difference (reference to input) to 90° phase difference. With the detector now operating to detect 90° out of phase response the phase was adjusted to zero response by adjusting a variable (0-100°) phasing control. Once zero response was obtained the phasing control was fixed and it was assumed that the lock-in amplifier/phase detector was locked to the square wave output and set up to detect 0° and 90° phase difference responses by means of changing the phase function switch. Each new modulation frequency required the above steps to be repeated to insure proper phasing.

The amplifier was checked in the range of frequencies from 1.5 Hz to 9000 Hz to test the flatness of the transmitted output. It was determined that there was no fall off in the transmitted output for the frequencies utilized. However the output was lower at frequencies above 3000 to 4000 Hz. Since the output appeared flat, it was fed to a recorder, Honeywell Electronik 193, and no adjustments were made to the readings from the recorder that otherwise would have had to be adjusted for fluctuations in transmitted power.

d. Honeywell Electronik 193 Strip Recorder

The output voltage from the PAR lock-in amplifier/phase detector was fed into the input voltage on the recorder. The zero scale point was adjusted so that both positive and negative deflections would be recorded. Recorder speed was normally set at 40 seconds/inch. Figure 18 is a sample of

the response recorded at 10 seconds/inch to give more clarity to the line shape of the response for comparison to figures 5 and 7. Normally 40 seconds/inch was used because the only data required was the peak to peak response.

e. Square Wave Generator

A Hewlett-Packard HP3300A Function Generator was used to supply the basic square wave modulation. A Beckman EPUT (Events Per Unit Time) Meter, model 6127, was utilized to give an accurate monitor of the actual modulation frequency supplied by the HP 3300A. The output from the HP 3300A was sent to the PAR lock-in amplifier/phase detector as the reference input and also supplied to a 1200 Volt silicon controlled rectifier (SCR) circuit. This circuit biased the square wave signal to a positive potential. This biased square wave was then amplified by a 0-1000 volt DC power supply and supplied the operating potential between the electrode and cavity walls. Another Tectronix type 503 oscilloscope was utilized to monitor the output voltage and display of the shape of the square wave output. A decreasing wave height (lowering voltage across the cavity) provided a means of detecting when an electrical short had developed between the center electrode and the cavity wall.

f. Princeton Applied Research, model 160, Boxcar Integrator

The Boxcar Integrator was used in place of the PAR lock-in amplifier/phase detector to obtain an accurate wave form recording of the response for estimating the relaxation time. Results using this are described in Section IVD.

4. Transmission Cavity Block Diagram

A block diagram of the equipment previously described is provided by figure 17. The hood arrangement and ZnO production was the same as explained in Section IIIC2, with the exception that the 1100° C furnace was replaced by the LINDBERG/HEAVIDUTY furnace, capable of producing 1500° C temperatures.

D. VARIABLES INVESTIGATED

The experimental investigations listed below were performed on the transmission experimental apparatus utilizing the final cylindrical coaxial cavity as described in Section IIIB3. The Response versus Applied E-field and Relaxation Frequency experiments were also investigated utilizing the rectangular cavities (reflection and transmission) however these experiments were rejected because of the problems encountered with the rectangular cavity designs and the superior results obtained with the cylindrical cavity.

1. Cavity Response versus Applied E-field

ZnO, produced at 1250° C, at a hydrogen flow rate of 24 ml/min, a nitrogen flow of 8.5 CFH, and an oxygen flow of 80 ml/min was introduced into the cylindrical coaxial cavity. A square wave modulation frequency of 31.7 Hz was applied to the cavity varying the amplitude of the applied modulated potential from 0 volts to 950 volts in increments of 50 volts.[1]

---

[1]For a discussion of the conversion of applied voltage to an average E-field strength given in Volts/cm, refer to Section IVA.

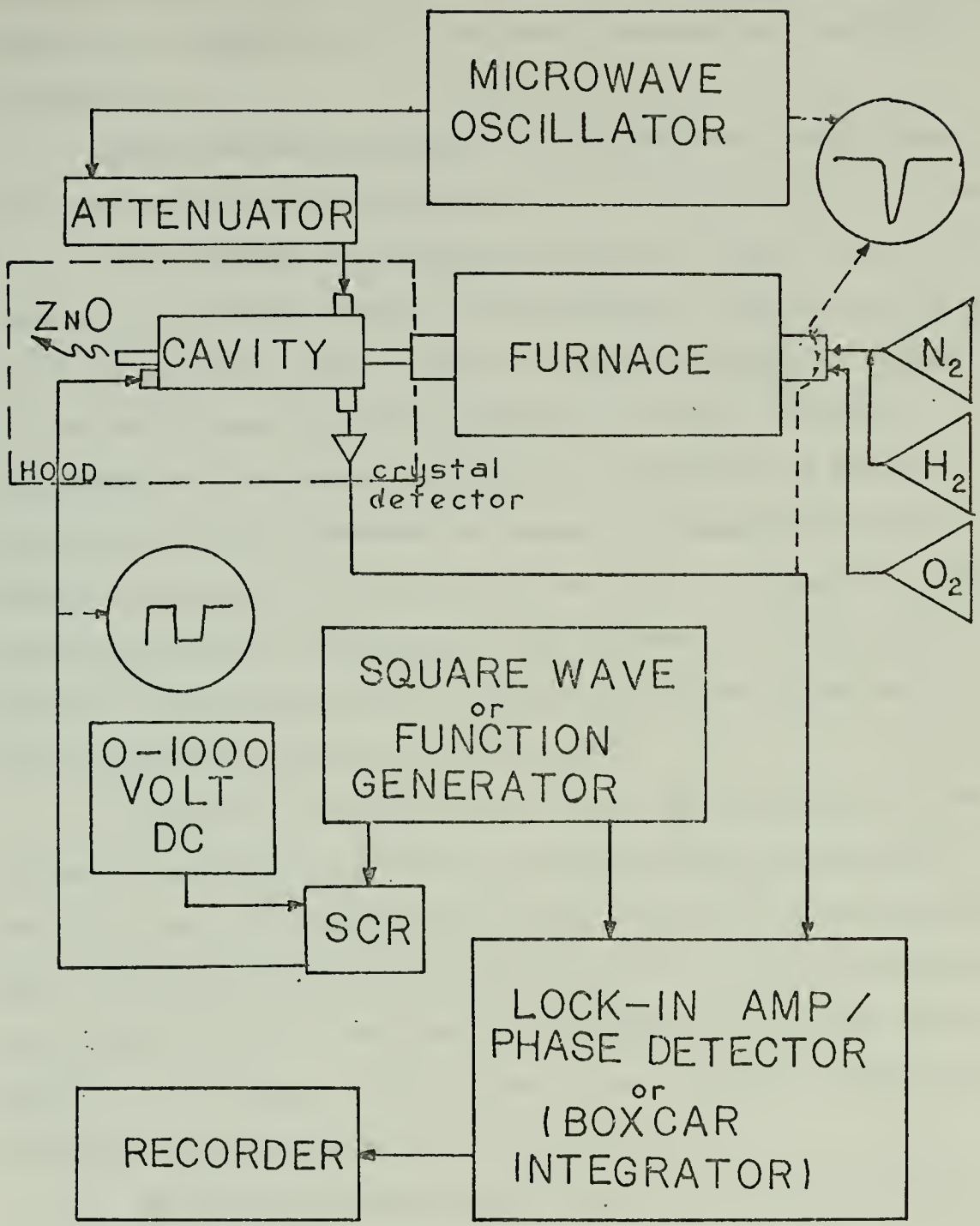

TRANSMISSION CAVITY APPARATUS

FIGURE 17

The PAR lock-in amplifier/phase detector was aligned as previously reported and the in-phase response was recorded exclusively.

When the sweep time on the HP8690B Sweep Oscillator was decreased to approximately 0.01 of the time used for the square wave determinations and the applied voltage was slowly (manually) increased from 0 to 950 volts, a sine wave modulation was applied to the cavity to obtain the rate of change of the cavity response versus applied E-field. For this determination the strip recorder was replaced by a Hewlett-Packard Mosley X-Y Recorder to record the magnitude of the change in response versus applied E-field. This method gives the derivative of the response with respect to the applied E-field. The results from this experiment are compared to the square wave results in Section IVB.

Since the size and shape of the ZnO particles in the effluent are highly sensitive to fluctuations in reactant gas flow rates, as reported by Vogel, et al, [7], a normalization to 300 Volts (190V/cm) was employed. The normalization was accomplished by performing a determination at 300 Volts (190V/cm) in between each voltage trial, thereby minimizing effects of changing ZnO particles with time.

2. Relaxation Frequency and Particle Size Distribution

For these investigations the in-phase and out-of-phase cavity responses were obtained utilizing the alignment procedures described earlier. These responses were obtained at various frequencies from 3 Hz to 400 Hz holding the applied

E-field at 190 V/cm. After each new frequency determination, a 31.7 Hz determination was taken so that the response could be normalized to this frequency to eliminate fluctuations in the response due to flow variations. Section IVD presents the results of these experiments.

3. Particle Characterization

a. Cavity Response vs Temperature (ZnO Production)

To classify the variable of temperature, fixed hydrogen, oxygen and nitrogen flows as reported previously were utilized while the temperature was varied from 1000° C to 1300° C. Particle samples were also collected at each temperature and scanning electron microscope photos of each were obtained to also show the variation of particle size and shape with temperature. These results are reported in Section IVF and figures 26, 27 and 28.

b. Cavity Response vs Reactant Gas Flow Rates

The in-phase response was recorded as the flow rate of first hydrogen then oxygen was varied. Results are reported in Section IVF and figures 29 & 30.

IV. RESULTS AND DISCUSSION

Section IIID provided a short introduction to the variables investigated, especially on saturation behavior and relaxation frequency investigations, to support the developed theory. Not included in any detail are the reasons for the decisions made to abandon an experimental apparatus or the problems encountered with specific methods. This section treats in greater detail the reasons why the evolution progressed in the manner in which it did.

The primary objective was to establish that the detected dielectric response was in fact a response produced by suspended particles. Evidence and conclusions establishing the fact that the observed response was from the suspended particles and supported the developed general theory is presented in the first two sections.

This basic response was then applied to saturation and relaxation frequency investigations to corroborate the theory developed in these areas and to serve as illustrations of some of the information which can be gained about particulate suspensions utilizing this method.

Finally, the characterization of the dependence of the response as a function of ZnO production parameters is presented. These determinations were in reality the first investigations performed because it was necessary to find the conditions which would produce the maximum enhancement of

the detected response so that a constant basis could be formed for evaluating the other investigations.

A. BASIC RESPONSE

The first attempts to observe and record the dielectric response by modulating between an aligned and non-aligned particle position were made with the reflection cavity and the Varian Unit. Attempts were made to record a response similar to that of figures 5 and 7 and to record a derivative response versus the applied electric field.

The reflection apparatus was discontinued due to several limitations which became evident after preliminary trials. These limitations were: (1) the ZnO particles introduced into the cavity rapidly accumulated in the cavity and degraded the response and finally led to a shorting of the applied potential, (2) the fixed iris coupling did not permit any flexibility in the amount of coupling of microwave energy into the cavity. This was a limitation because the cavity response could not be adjusted to provide a consistent basic cavity resonance condition and finally, (3) the system was basically designed to employ a sine wave modulation and produce a derivative response; however, a derivative response is characteristically less sensitive than the direct response. These facts coupled with a low Q cavity led to a response which was extremely noisy.

The second attempt employed a square wave modulation, giving a direct as opposed to the derivative response, a higher Q transmission cavity with a variable coupling feature

and larger volume (6 cm in length versus the 5 cm reflection cavity) so that particle build up would not occur as rapidly as in the reflection cavity.

Using the square wave and varing the modulation amplitude from zero to the voltage applied, the rectangular transmission cavity was utilized with the equipment described in Section IIIC3 to obtain the desired response. A response similar in form to that described by figures 5 and 7 was obtained. Attempts to classify this response by recording the magnitude of the response versus the applied E-field to confirm saturation behavior were only partly successful. When the voltage was reduced to zero the response dropped to zero; however, when the ZnO production was stopped, allowing only nitrogen gas to enter the cavity, and with the E-field modulation still applied to the cavity, a considerable response remained.

It was concluded that as the ZnO particles were introduced into the cavity some of the particles would precipitate out of the suspension and adhere to the cavity walls and plate. These particles tended to build up along the applied E-field lines from the plate to the cavity walls and effectively formed very large particles. Since the TE_{102} mode E-field patterns are strong at the position of the plate, the "stuck" particles contributed significantly to the observed response. Corrections to the observed data could have been applied; however, in order to apply an accurate correction, a zero ZnO flow response would have to be made for each voltage determination. This in itself would lead to other more

serious problems because of the sensitivity in the response exhibited by the ZnO to fluctuations in flow rates of the reactant gases. Figures 29 and 30 illustrate the change in the response with changing hydrogen and oxygen flow rates. For an experimental determination to have meaning, it would require an ability to accurately return to fixed, constant hydrogen and oxygen flow rates so that the ZnO produced would respond in a predictable manner. The flow meters available were not accurate enough to meet the standards imposed by this requirement; therefore, the responses recorded from the rectangular transmission cavity had an intrinsic error of variable magnitude. It may be possible to utilize a rectangular cavity for these measurements if it can be established that the "stuck" particle response is a given percentage or some known or determinable function of the total response for a given E-field strength and modulation frequency. The necessity for defining such a correction function was circumvented in this study by searching for a suitable cavity design for which resonant modes exist that do not have strong microwave E-fields at potential particle accumulation sites.

The field configurations listed by Ginzton [14] for a coaxial transmission line show that the TE_{01} mode supplies the required microwave E-field pattern. Assuming that the cavity described in Section IIIB3 is a coaxial cylindrical cavity, the TE_{012} mode was chosen as the cavity mode of operation. The E-field lines in this mode are concentric with the coaxial cylinders and diminish to zero at both the

inner rod and outer wall. If the modulated E-field is applied from inner rod to outer wall, the response will be that of aligning the particles perpendicular to the microwave E-field. This response should conform to the predicted response of F(E) in Section IB. This method has the effect of lowering the overall sensitivity of the system by a factor of two because of the randomness of the particle alignment parallel to the microwave E-field when the applied E-field is zero. However, any "stuck" particles will be aligned perpendicular to the microwave E-field making negligible contribution to the observed response; and, the accumulation of precipitated particles takes place in a region of low microwave E-field intensity. These factors effectively eliminated the problem of the precipitated particles, and provided a means of measuring the effects produced by the suspended particles only. As a check that the "stuck" particle problem was solved, ZnO production was stopped and an E-field applied to the cavity. The response dropped to zero as the ZnO production was stopped. As a further indication that the observed response was from suspended particles, the oxygen flow was decreased allowing a higher percentage of metallic zinc to accumulate on the ZnO particles producing an effective particle of increased conductivity. When the oxygen flow was stopped meaning that ZnO was no longer being produced the response dropped to zero; however, if accumulated particles had been contributing to the response, there would have been a response for the zero ZnO production.

The cylindrical coaxial cavity was the cavity utilized to verify and characterize the particle response. The externally applied E-field strength for this cavity is not constant but shows a 1/radius type dependence as stated previously. This calculation was performed assuming coaxial geometry and applying Green's theorem to a Gaussian surface parallel to the cavity walls. In order to account for the variation in the applied E-field strength and the variation in microwave E-field strength, it was necessary to calculate an effective spacing between the inner rod and outer wall to determine an average E-field strength. From the Green's theorem calculation:

$$E = \frac{k}{r} \quad , \quad k = \text{a constant} \tag{22}$$

The applied potential difference is:

$$V = - \int_{r_2}^{r_1} E \cdot dr$$

where r_1 and r_2 are the inner and outer wall radii

Upon substitution of E, solving for k, and replacing k in Equation 22 yields:

$$E = \left[\frac{V}{\ln(r_2/r_1)}\right] \left(\frac{1}{r}\right)$$

The average E-field value, <E>, is

$$\langle E \rangle = \frac{V}{\ln \frac{r_2}{r_1}} \frac{\int_{r_1}^{r_2} \frac{r}{r} \sin^2[\pi \frac{(r-r_1)}{(r_2-r_1)}]\, dr}{\int_{r_1}^{r_2} r \sin^2[\pi \frac{(r-r_1)}{(r_2-r_1)}]\, dr}$$

where the averaging process accounts for the applied E-field (1/r) and the microwave E-field ($\pi(\frac{r-r_1}{r_2-r_1})$). Upon substituting $u = \frac{\pi(r-r_1)}{(r_2-r_1)}$

$$\langle E \rangle = \frac{V}{\ln \frac{r_2}{r_1}} \frac{\int_0^{\pi} \sin^2 u\, du}{\int_0^{\pi} r \sin^2 u\, du}$$

$$\langle E \rangle = \frac{V}{\ln \frac{r_2}{r_1}} \left(\frac{1}{\frac{r_2+r_1}{2}} \right) \qquad (23)$$

Therefore the average E-field strength is the value of the E-field evaluated at the middle of the spacing between the inner and outer walls. For the cylindrical coaxial cavity with r_1 = 1.2 cm and r_2 = 2.7 cm an effective spacing of 1.581 cm was calculated from equation 23. The E-field strength in Volts/cm then is equal to the applied voltage divided by 1.581.

Figures 18 a, b, and c show the recorded responses from zinc oxide particles produced at 1250° C. The cylindrical cavity microwave resonance was at 11.35 GHz with a 500V

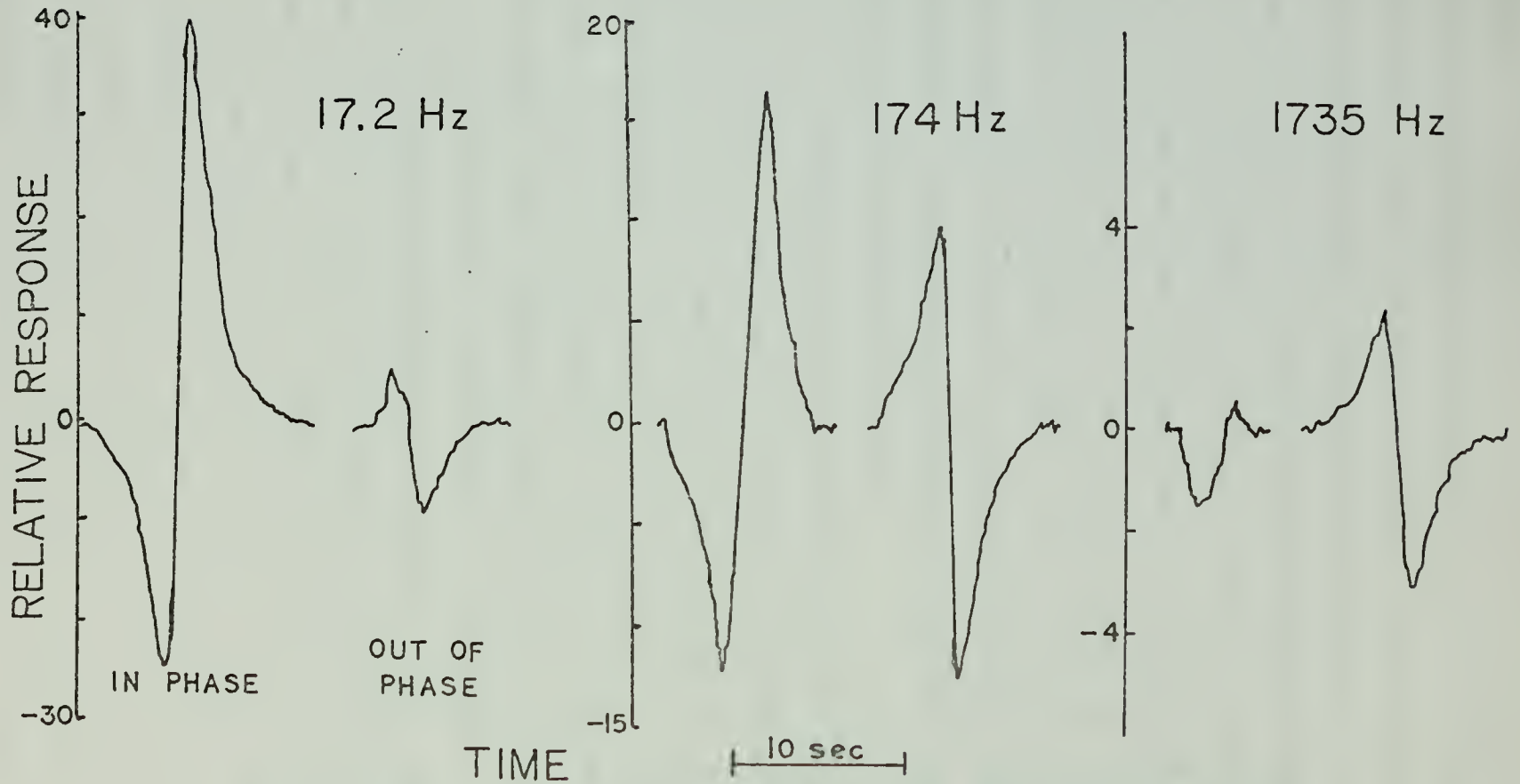

IN-PHASE AND OUT-OF-PHASE RESPONSE OF
ZnO PRODUCED AT 1250°C (500 V
SQUARE WAVE)

FIGURE 18

potential modulated at 17.2, 172 and 1735 Hz (square wave) applied from inner rod to outer wall. The in-phase response was taken as the 0° phase difference from reference output from the PAR Lock-in Amplifier/Phase Detector and the out-of-phase response as the 90° phase difference response. The relative amplitude (peak to peak) for the in-phase response was utilized as the response for the saturation behavior investigation and as the real response in the relaxation and particle size determinations. The out-of-phase response was only used in the particle size determination as the imaginary response. These investigations are presented in greater detail in Sections IVD and IVE.

The recorded responses are shown versus time. This time is related to the microwave frequency by the sweep speed, center frequency, and sweep width used on the HP8690B Sweep Oscillator. For the investigations performed in this study, it was not necessary to make the conversion since only the peak to peak amplitude was utilized as the cavity response.

To illustrate to some extent the difficulties encountered with changing ZnO production, figure 19 is a comparison of the in-phase response recorded for ZnO particles produced from the same ZnO core, doped with 0.05° mole % In, under equivalent reactant gas flow conditions and a modulation frequency of 31.7 Hz. The two responses were recorded six days apart. During this interval the ZnO core remained in the furnace at 900° C. The furnace temperature was increased from 900° C to 1250° C for the particulate suspension production.

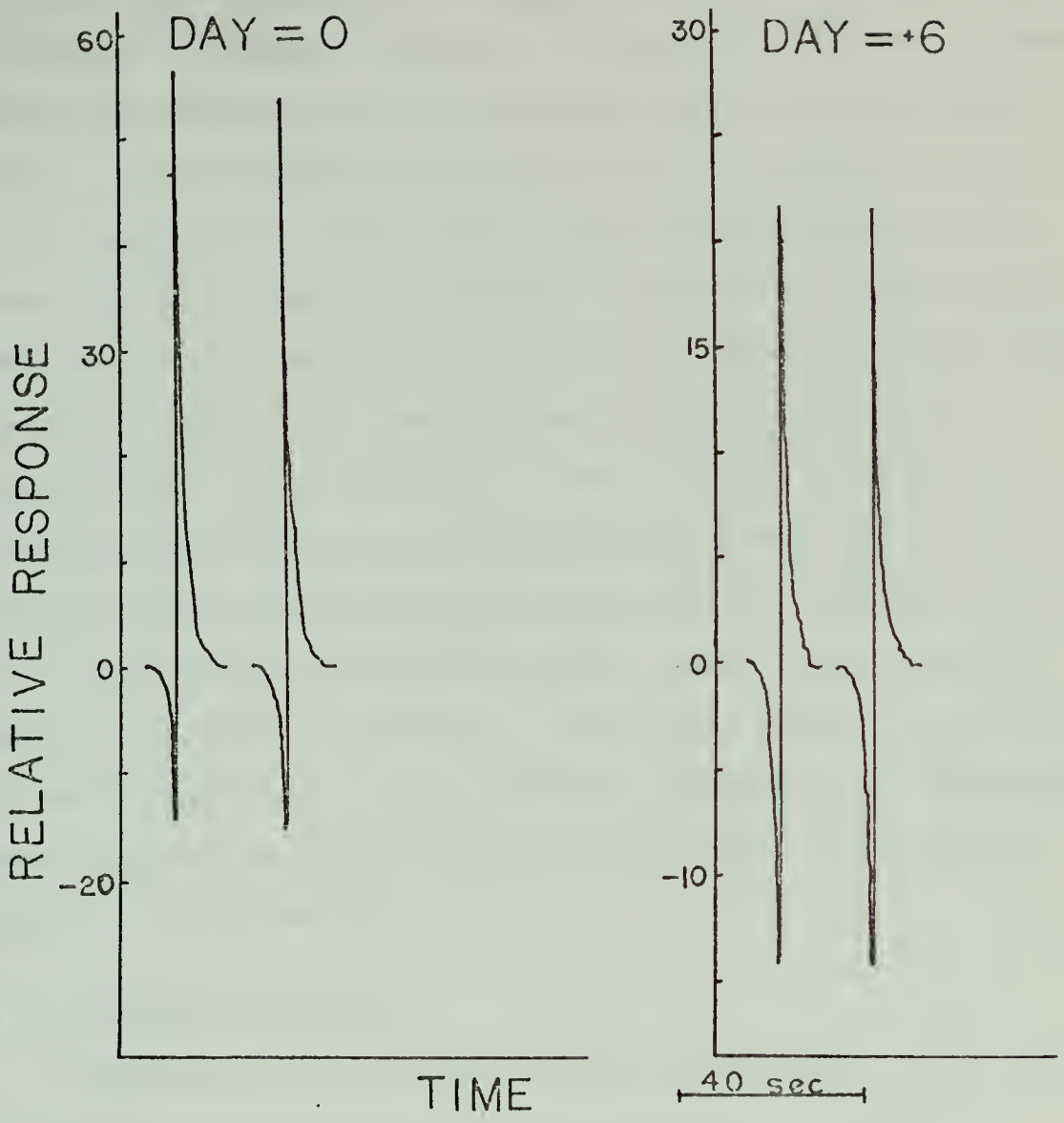

EFFECT OF AGING ON IN PHASE RESPONSE

FIGURE 19

If these two responses are compared to figure 7 which illustrates the predicted response line shape for different percentage real responses, the particles produced from the ZnO core the longer the core had remained in the furnace showed an increased real (less lossy) response which may be the result of core "aging" or slight fluctuations in the reactant gas flow conditions or a combination of these effects. This apparent change with time of the core and the sensitivity of the response to fluctuations in reactant gas flow rates made it necessary to perform an experimental investigation continuously without stopping particle production, changing production temperature or gas flow rates. These principles were employed as much as possible. To further negate the effects of the fluctuations in the response normalization techniques were employed for the saturation behavior and relaxation frequency experiments.

B. DERIVATIVE RESPONSE

In addition to the basic response from square wave modulation at a fixed electric field strength, a derivative response was obtained using a sine wave and manually varying the E-field strength applied to the cavity. The strip recorder was replaced with an x-y recorder and the sweep time on the sweep oscillator was decreased to 0.01 of the time utilized for the square wave. Figure 20 illustrates the derivative response obtained utilizing the cylindrical coaxial cavity and 100 Volt, peak to peak, sine wave modulation at 31.7 Hz. A silicon controlled rectifier circuit, Section IIIC3e,

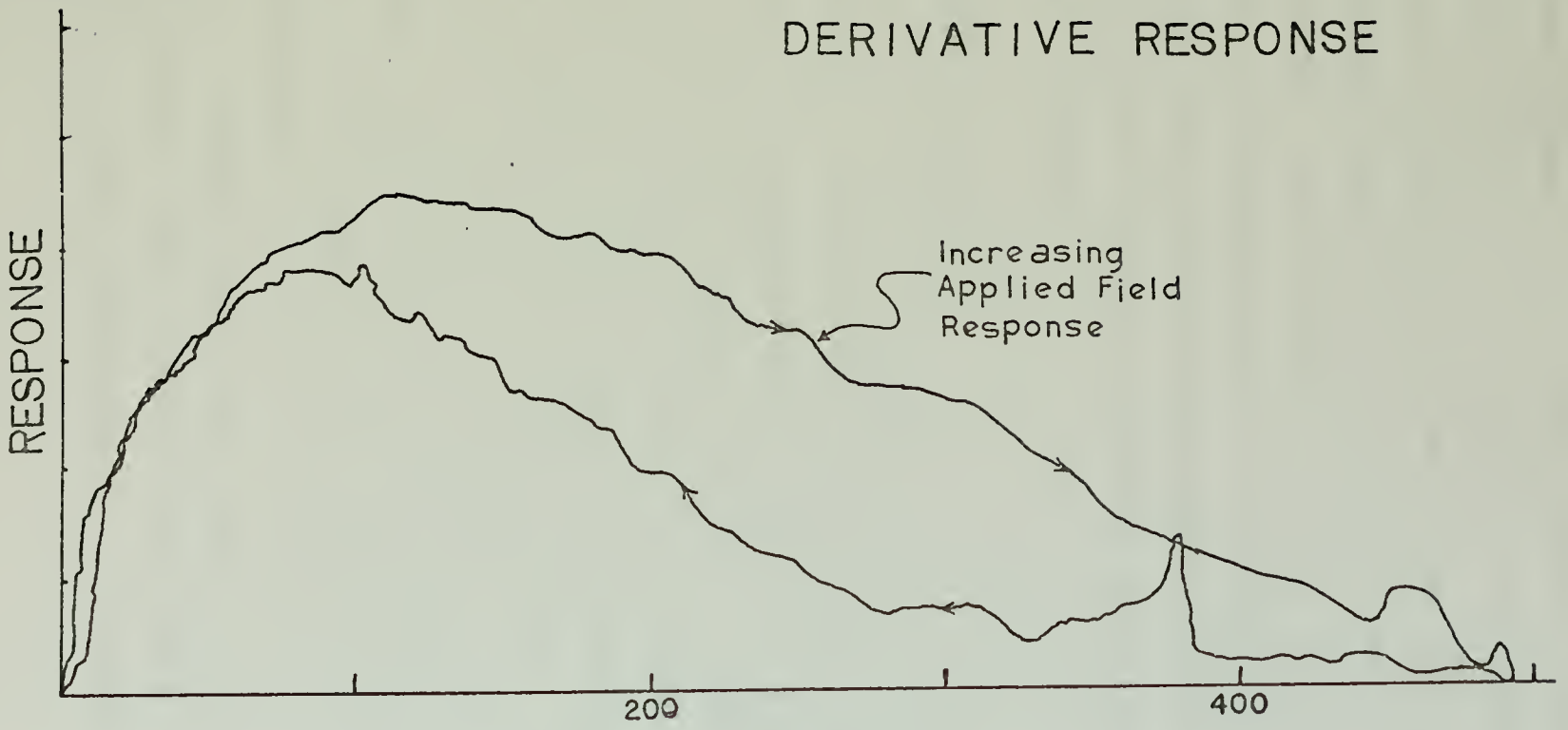
DERIVATIVE RESPONSE
RESPONSE
Increasing
Applied Field
Response
200
400
APPLIED E-FIELD

FIGURE 20

provided a positive bias to the sine wave; however, the non-linear effects of the circuit produced a hysteresis phenomenon in the recorded output as indicated by the different paths for increasing and decreasing applied E-field. For computational purposes the increasing E-field response curve was utilized. The normalized integrated response using this technique is presented in the following section along with the square wave response and predicted saturation curves to characterize the saturation behavior exhibited by the ZnO particles produced.

C. SATURATION BEHAVIOR

In Section IIB a development was given for the predicted response that non-spherical particles should exhibit when subjected to an applied electric field. The response, f(E), versus A was shown in figure 8 where $A = \sqrt{\frac{\alpha}{2kT}}\, E$. A development was also presented for F(E), the response predicted for particles being deflected away from the applied field which is the cylindrical coaxial cavity situation. If the values of F(E) for increments in A from Table II are plotted the resultant curve would predict the cylindrical cavity response versus A or the response versus applied E-field if $\frac{\alpha}{2kT} = 1$. The E-field has to be given in statvolts/cm to conform to the e.s.u. cgs units used with equation 16 for the approximate value of α. The saturation investigations which were performed measured the response as a function of the applied field.

Two methods, the direct and the derivative response, were utilized to characterize the saturation behavior of the ZnO particles produced. Particle samples were collected while the experiments were in progress and allowed to precipitate onto metal discs so that scanning electron microscope (SEM) photographs could be obtained. From these photographs the particles were estimated to be approximately three microns in length and have an effective length to diameter ratio of approximately 40.

Figure 21 presents the direct results obtained using a 31.7 Hz square wave modulation and increasing the applied E-field from 0 to 600 Volts/cm (0 to 2 Statvolt/cm). The responses were normalized to 190 Volts/cm to eliminate the effects of changing ZnO production as explained previously. The solid line in figure 21 is the predicted response versus applied E-field obtained from F(E) vs A by multiplying the A values from Table II by a scale factor of 1.7 and the F(E) values by a scale factor necessary to expand the F(E) values to conform to the normalized response.

From the scale factor of 1.7 a value for α was obtained because the graphical limits were set up so that when A = 6 X 1.7 = 10.2, E = 2 Statvolt/cm = 600 V/cm therefore:

$$A = \beta E \quad , \qquad \text{where } \beta = \frac{\alpha}{2kT}$$

$$\beta = \frac{A}{E} = \frac{10.2}{2} = 5.1 = \frac{\alpha}{2kT}$$

FIGURE 21

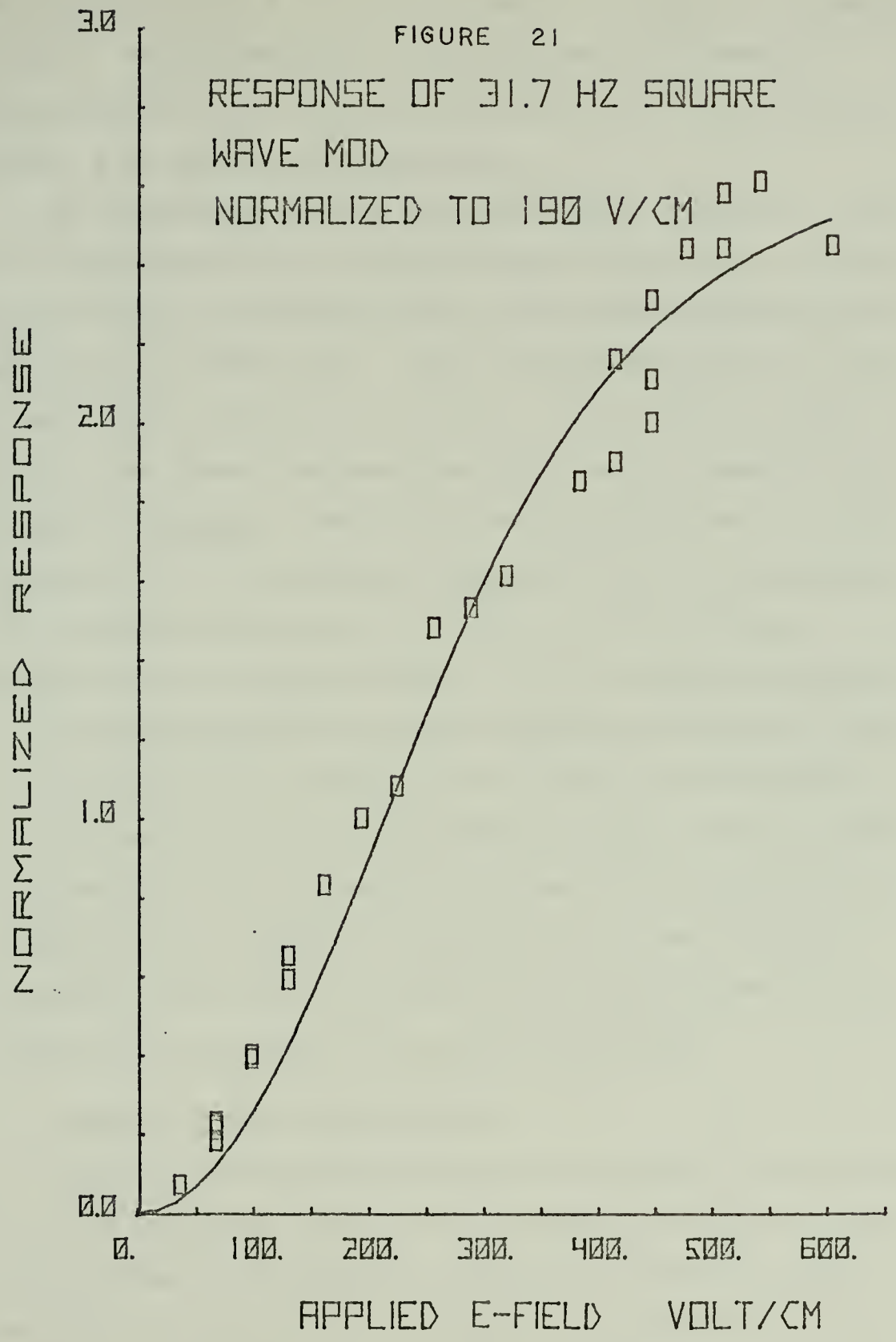
RESPONSE OF 31.7 HZ SQUARE
WAVE MOD
NORMALIZED TO 190 V/CM
NORMALIZED RESPONSE
3.0
2.0
1.0
0.0
0.
100.
200.
300.
400.
500.
600.
APPLIED E-FIELD VOLT/CM

which yields an $\alpha \tilde{=} 2.15 \times 10^{-12}$ cm^{-3}. A length to diameter ratio of 40 was assumed for the ZnO particles produced. From equation 16 an effective particle size, ℓ, of approximately 2.16 microns was calculated.

The increasing applied field derivative response, figure 20, was integrated on a Hewlett-Packard Model 9100A Calculator utilizing the Simpson's Rule Integration program available with the Model 9100. This integrated response, normalized to the 190 Volt/cm response, is presented in figure 22. As with the direct response the solid curve represents the predicted response. The scale factor multiplying A in this instance is 1.25. Using the same development as presented for the direct response an $\alpha \tilde{=} 1.16 \times 10^{-12}$ cm^{-3} and a particle size of approximately 1.76 microns was calculated.

This development has characterized the saturation behavior of ZnO particles and provides a means for determining the average size of the suspended particles. The following sections provide other means for size and size distribution determinations along with characterizing other important parameters such as the relaxation time and frequency associated with the size of the particle produced.

D. RELAXATION TIME AND FREQUENCY

Figure 9 from Section IID which illustrates the predicted real and imaginary response from equation 20 can be utilized to determine the relaxation frequency directly. In order to verify the predicted line shape an investigation of the in-phase response measured at increasing modulation frequencies

FIGURE 22

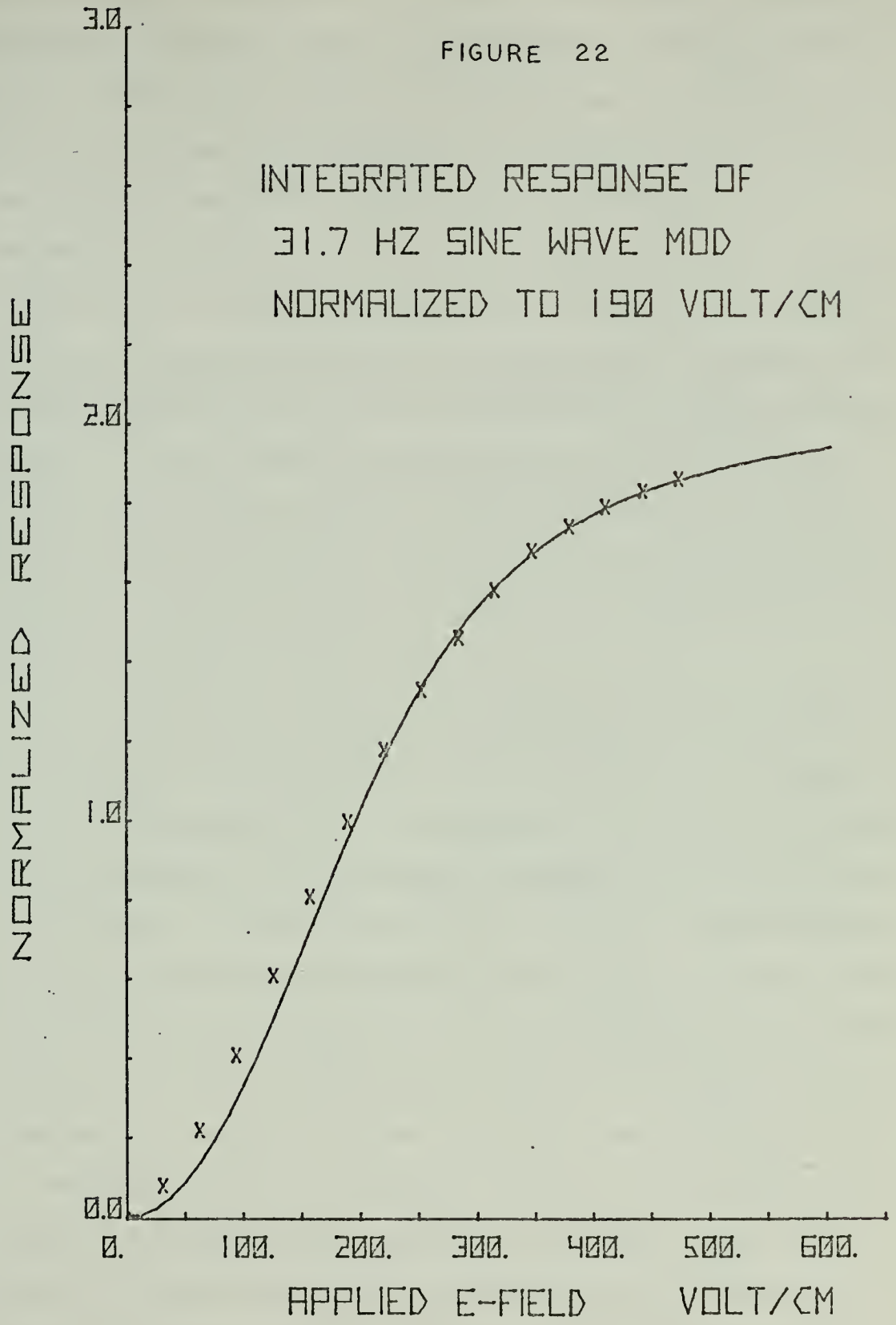
INTEGRATED RESPONSE OF
31.7 HZ SINE WAVE MOD
NORMALIZED TO 190 VOLT/CM
NORMALIZED RESPONSE
3.0
2.0
1.0
0.0
0.
100.
200.
300.
400.
500.
600.
APPLIED E-FIELD VOLT/CM

was performed. Figure 23 is a plot of both the real and imaginary response obtained as explained in Section IIIC3c and at frequencies from 3 to 400 Hz using a 300 Volt square wave. The square wave magnitude of 300 Volts (190 Volt/cm) was chosen because the response at this voltage is not saturated. As explained before a normalization was required to negate the effects of changing ZnO production. In this case 31.7 Hz was chosen as the normalization frequency and a determination at 31.7 Hz was performed after each new frequency. It was noted that highly divergent data points resulted for those frequency determinations for which the before and after 31.7 Hz response did not remain approximately constant. These results were rejected as being spurious and are not included in figure 23.

The relaxation frequency was taken as the point where the in-phase response had fallen to one half its original value (0 Hz modulation). A frequency of 56 Hz was determined to be the approximate relaxation frequency for the ZnO particles produced. However this 56 Hz is only an approximation due to the scatter in the data and the range of values possible because of the log plot for small variations in the determination of the one half response point. The shape of the experimental curve does show in general the same shape for the real portion of the response function as illustrated by figure 9. From SEM photographs, figure 24a, of the ZnO particles produced during this investigation an average effective particle size of approximately 2.8 microns was

FIGURE 23

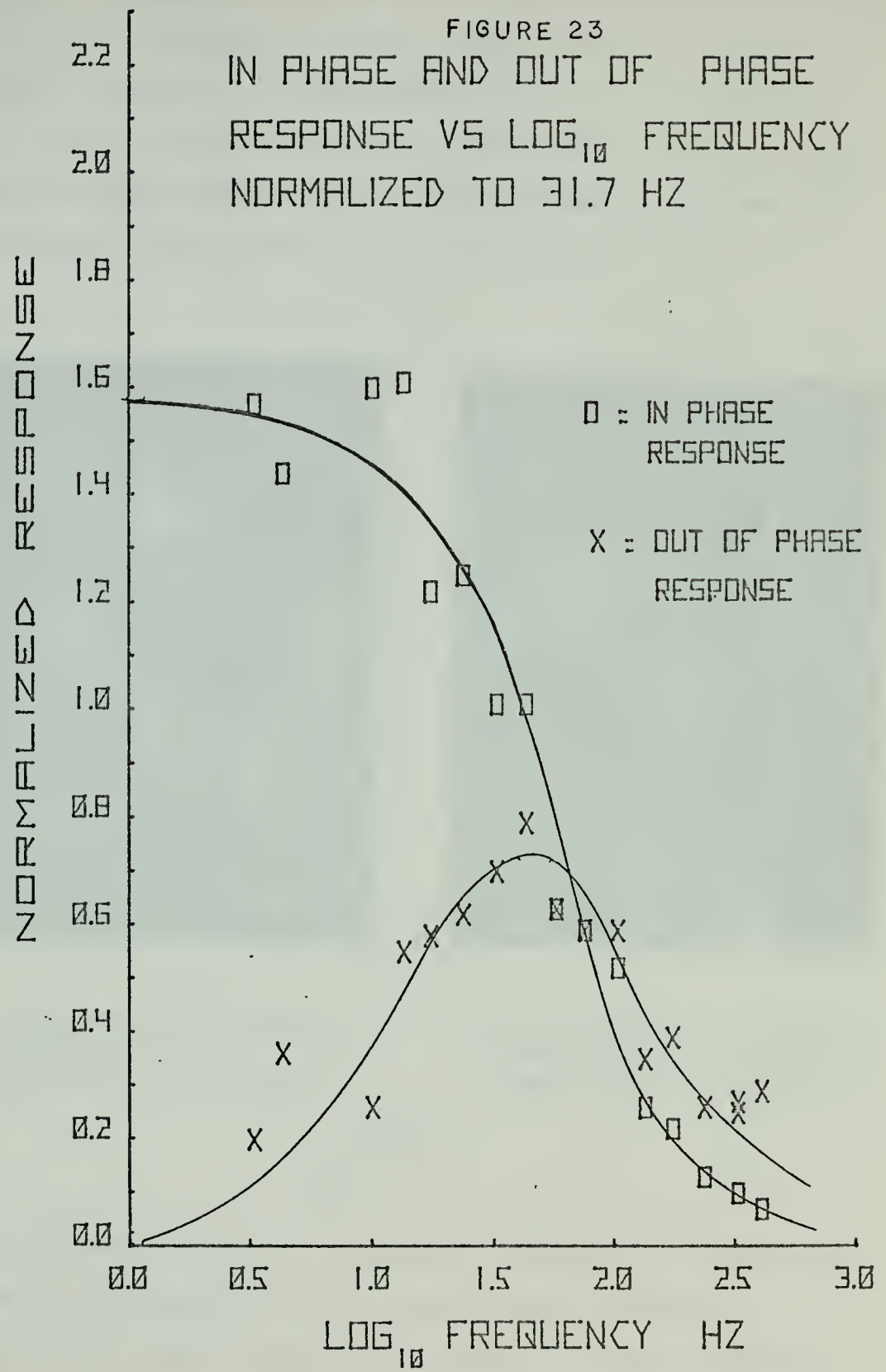
IN PHASE AND OUT OF PHASE
RESPONSE VS LOG10 FREQUENCY
NORMALIZED TO 31.7 HZ
NORMALIZED RESPONSE
2.2
2.0
1.8
1.6
1.4
1.2
1.0
0.8
0.6
0.4
0.2
0.0
0.0
0.5
1.0
1.5
2.0
2.5
3.0
LOG10 FREQUENCY HZ
□ : IN PHASE RESPONSE
X : OUT OF PHASE RESPONSE

obtained. The predicted relaxation frequency for a particle size of 2 to 4 microns from Table III is from 170 to 24 Hz. Also from Table III the experimental frequency of 56 Hz yields a particle size of slightly less than 3 microns, thus the experimental results are in good agreement with the size particles estimated from the SEM photographs.

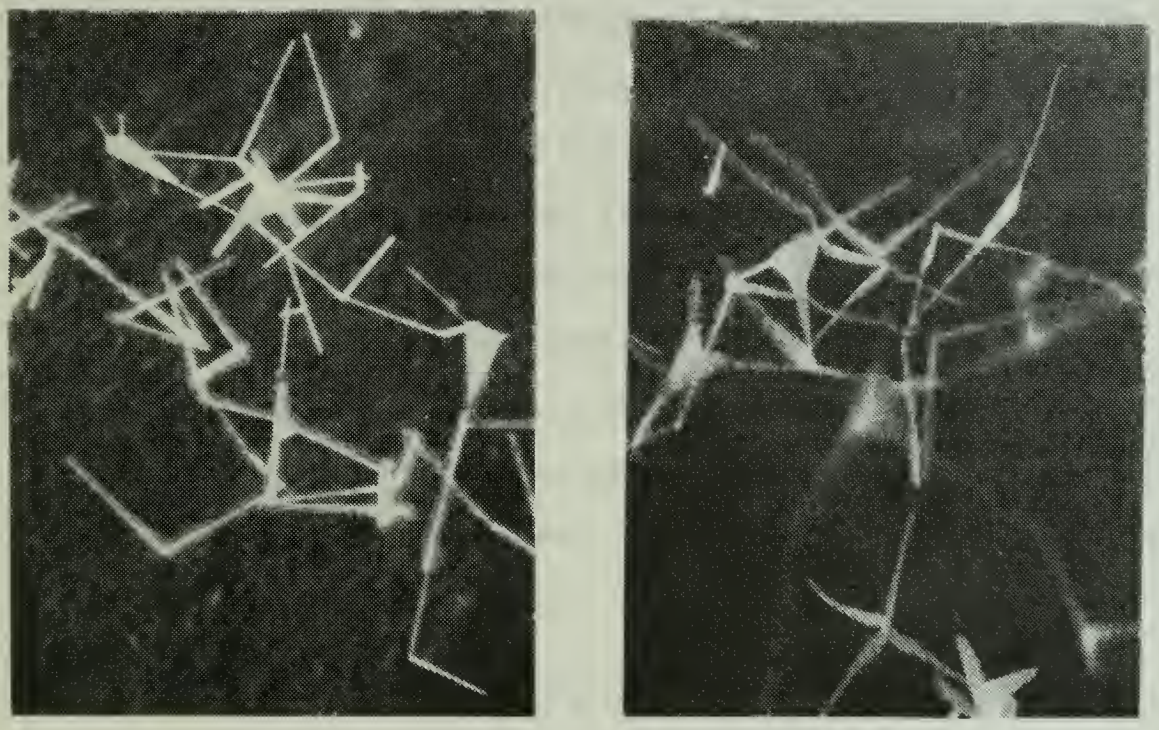

(a)
ZnO Particles Produced during Relaxation Investigation (1250°C)

(b)
ZnO Particles Produced during Boxcar Integrator Investigation (1250°C)

1μ

Figure 24

To further define the relaxation frequency the PAR Boxcar Integrator was inserted in the experimental apparatus, Section IIIC3f, and a plot of the applied waveform obtained,

figure 25. The relaxation time was taken as the time required for the exponential decay to fall to 1/e of its maximum value. From figure 25 a relaxation time of approximately 2.1 X 10^{-3} sec was obtained. The relaxation frequency was then calculated from equation 19 to be approximately 75 Hz.

Again from Table III, 75 Hz corresponds to a particle size between 2.5 and 3.0 microns. The Boxcar Integrator investigations were not performed on the same day as the previous experiment. The fluctuations due to possible core changes could account for the difference in relaxation frequencies observed. However from SEM photographs, figure 24b, the ZnO particles produced during the Boxcar Integrator investigations had an estimated average particle size of approximately 2.5 microns. The relaxation time corresponding to the 56 Hz determined relaxation frequency is 2.8 X 10^{-3} sec and is in good agreement with the 2.1 X 10^{-3} sec obtained from the Boxcar Integrator.

E. PARTICLE SIZE DISTRIBUTION

The out-of-phase response (Imaginary) was plotted on the same graph as the in phase response, figure 23. This response also followed the general form predicted by figure 9. The ratio of the peak imaginary response to the peak real response was estimated to be 0.48. From Table IV a ratio of 0.48 yields a σ of approximately 6.3. By substitution of $\sigma = 6.3$ into: $\sigma(\ln \tau/\tau_o)^2 = 1$

$$\ln \tau/\tau_o = 0.398$$

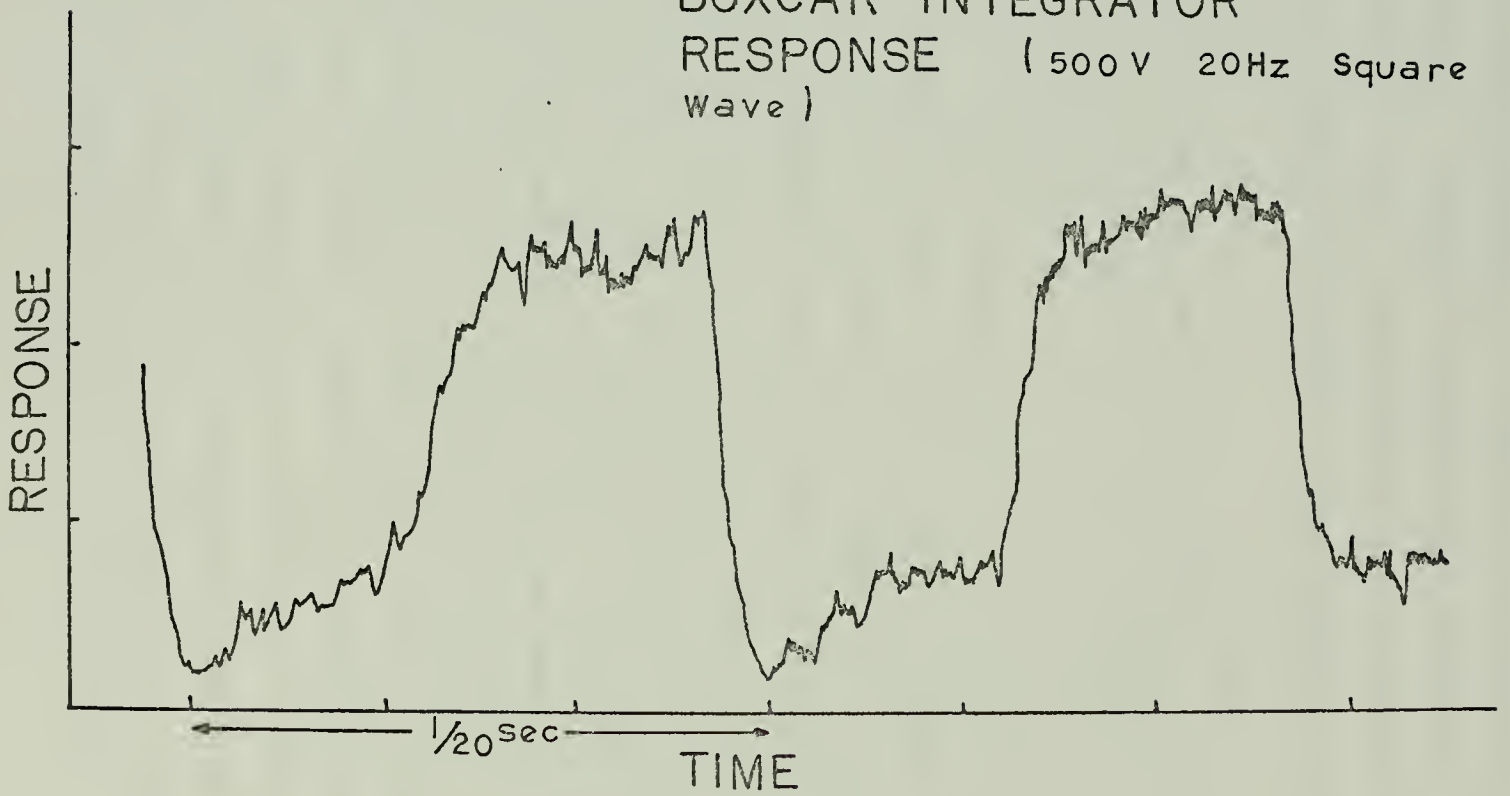
BOXCAR INTEGRATOR
RESPONSE (500V 20Hz Square Wave)
RESPONSE
1/20 sec
TIME

FIGURE 25

Therefore the width of the distribution in τ values will be from 0.601 τ_o to 1.398 τ_o. If τ_o is taken to be 2.45 X 10^{-3} sec which is the average of the relaxation times from the in phase response and the Boxcar Integrator investigations then the distribution in τ values would be from 1.47 X 10^{-3} sec to 3.42 X 10^{-3} sec. By a comparison of the τ values to the particle sizes in Table III these τ values infer a particle size, L, of $2\mu < L < 3.5\mu$.

The particle sizes as used in the foregoing development are in reality effective particle sizes. The effective particle size was assumed to be the tip to tip distance of adjacent legs of the fourling and not the total particle size measured along the legs. It was further assumed that there were a sufficient number of non-symmetrical particles i.e., broken or fragmented fourling structures, present in these samples to account for the observed response.

In Section IIIA it was mentioned that two different ZnO cores were used for particle production. In the original determinations using the reflection and transmission cavities, ZnO cores with 0.05 mole % In doping were utilized. A series of trials were conducted with the reagent grade ZnO cores and the cylindrical cavity; however, the results from these trials were irratic and could not be repeated or reproduced to any degree of accuracy. The response was strongly degraded for the reagent grade ZnO core when compared to the response obtained under similar conditions with the In doping. The

doped samples did not appear to be different from the reagent ZnO with respect to size or fourling formation.

The increased conductivity of the indium doped samples may account for the difference in the magnitude of the observed response because of the subsequent increase in the polarizability. Without exception the results reported were those obtained with the doped ZnO cores.

F. PARTICLE CHARACTERIZATION

1. Response versus Temperature (ZnO Production)

To obtain the maximum response from the ZnO particles, the response was measured as the ZnO production temperature was increased. Figure 26 illustrates the relative response of the ZnO particles as the temperature at which the particles were produced is increased. Reactant gas flow rates were held constant at 26 ml/min hydrogen and 85 ml/min oxygen. Particle length as a function of production temperature is presented in figure 27. These particle lengths were determined from SEM photographs, figure 28, of particles collected at each temperature. The greatest response was recorded at 1250° C. It was for this reason that the investigations of saturation and relaxation behavior were carried out at this temperature.

2. Reactant Gas Flow Rates

As previously noted the response exhibited by the ZnO particles was highly sensitive to fluctuations in gas flow rates. Figure 29 shows the dependence of the response on hydrogen flow rates holding the oxygen flow rate constant

FIGURE 26

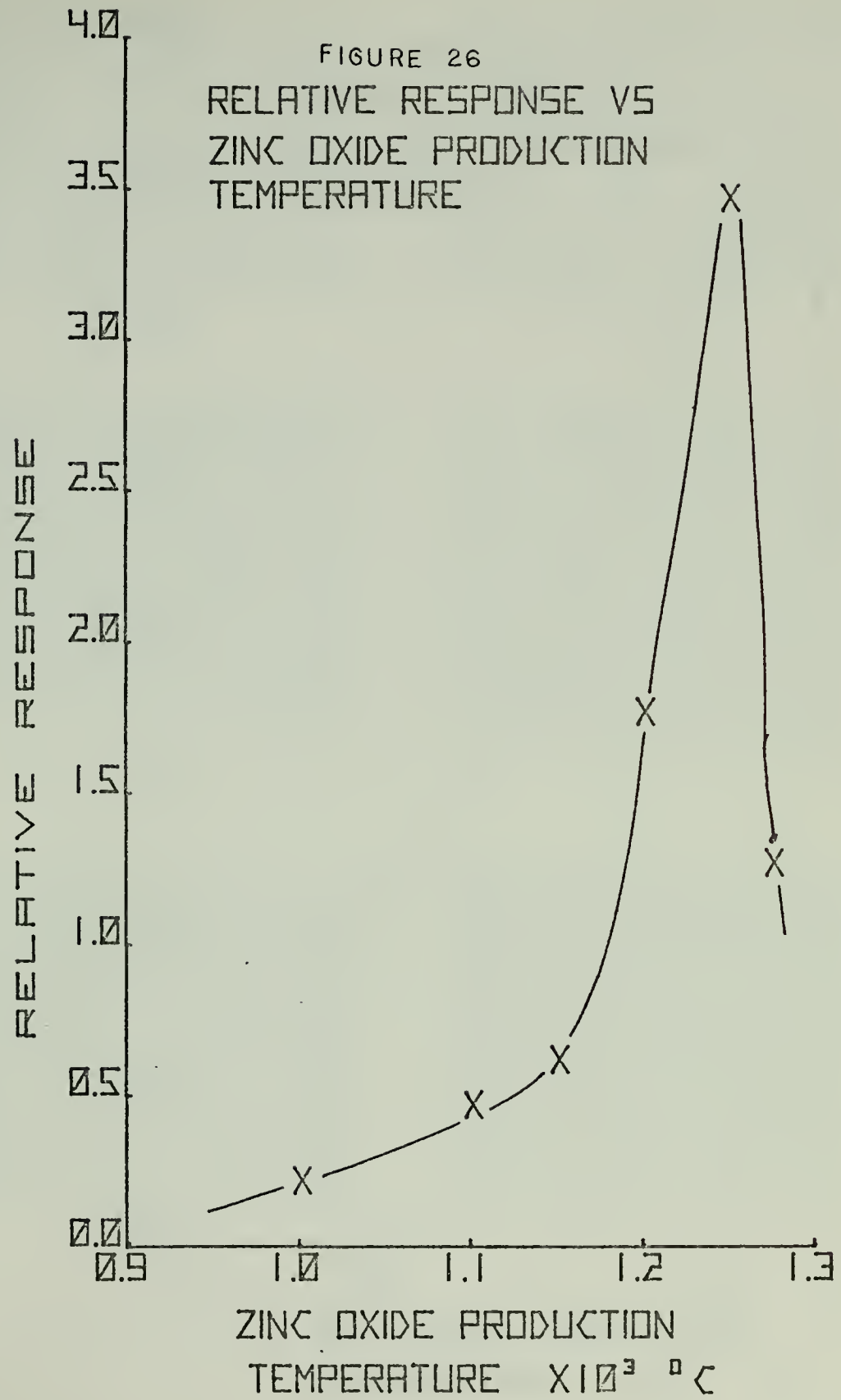
RELATIVE RESPONSE VS
ZINC OXIDE PRODUCTION
TEMPERATURE
RELATIVE RESPONSE
4.0
3.5
3.0
2.5
2.0
1.5
1.0
0.5
0.0
0.9
1.0
1.1
1.2
1.3
ZINC OXIDE PRODUCTION
TEMPERATURE X10³ °C

FIGURE 27

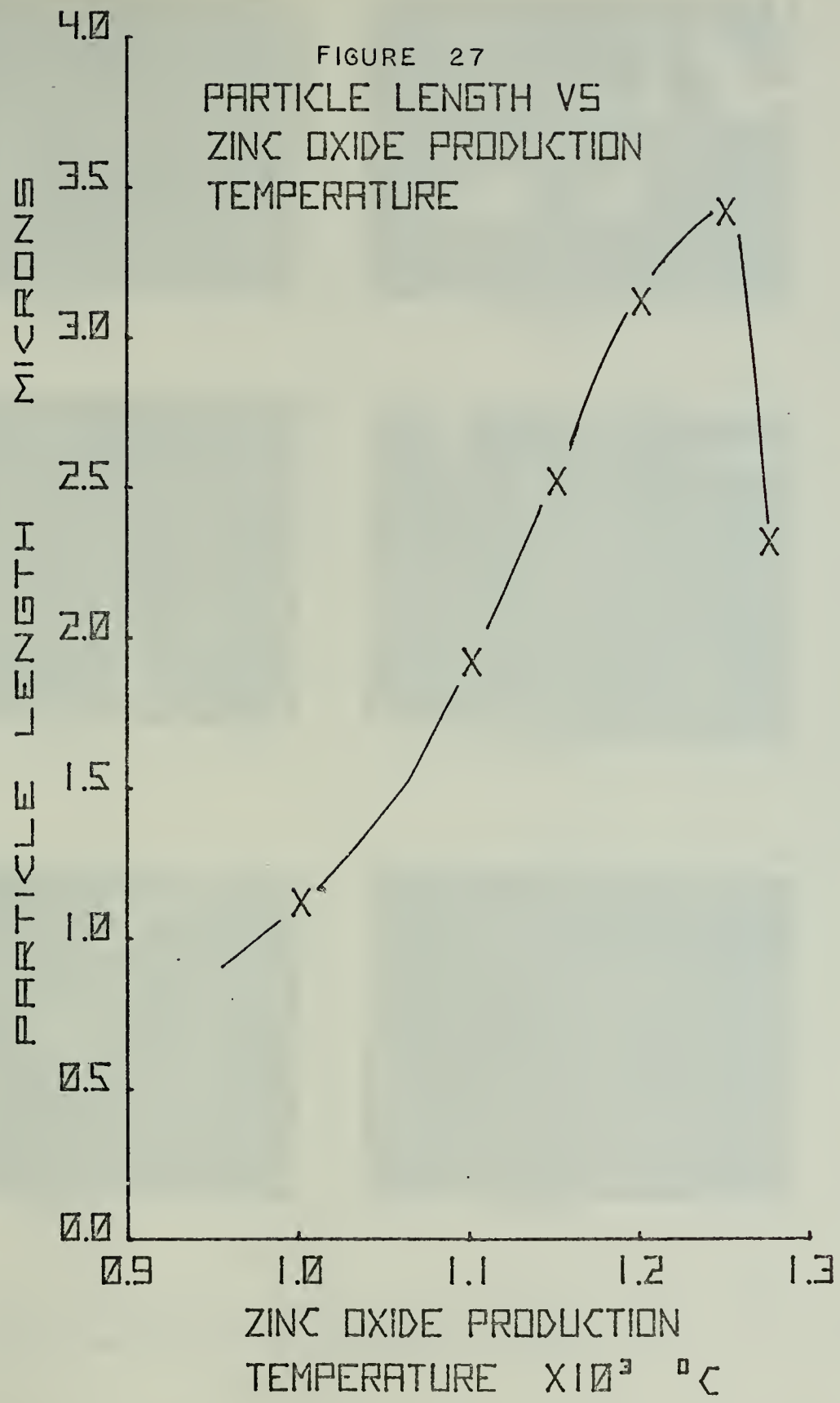
PARTICLE LENGTH VS
ZINC OXIDE PRODUCTION
TEMPERATURE
PARTICLE LENGTH MICRONS
4.0
3.5
3.0
2.5
2.0
1.5
1.0
0.5
0.0
0.9
1.0
1.1
1.2
1.3
ZINC OXIDE PRODUCTION
TEMPERATURE X10³ °C

1000°C

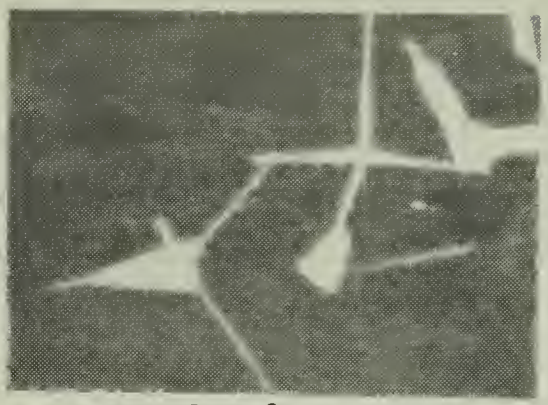

1200°C

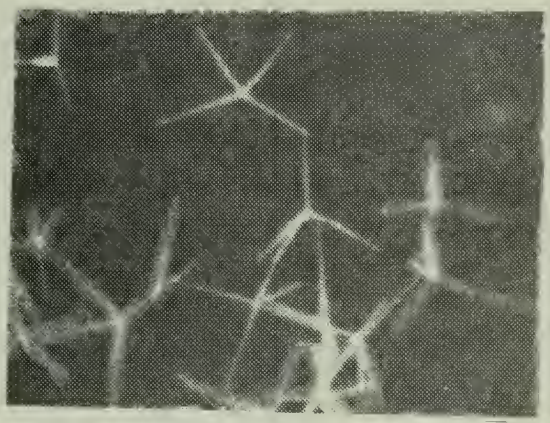

1100°C

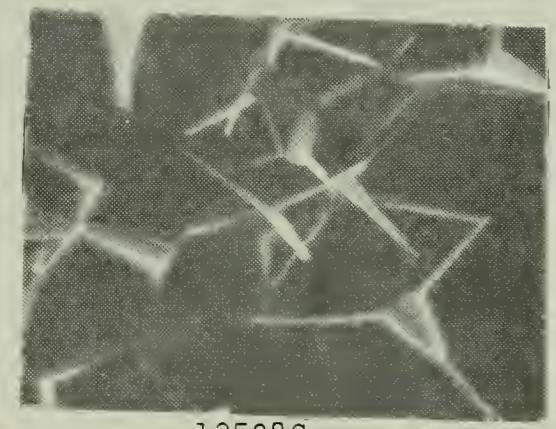

1250°C

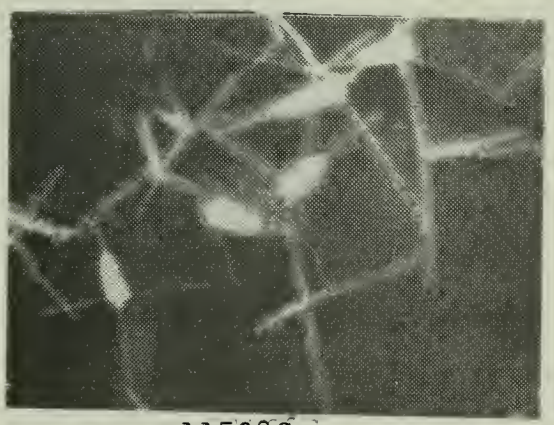

1150°C

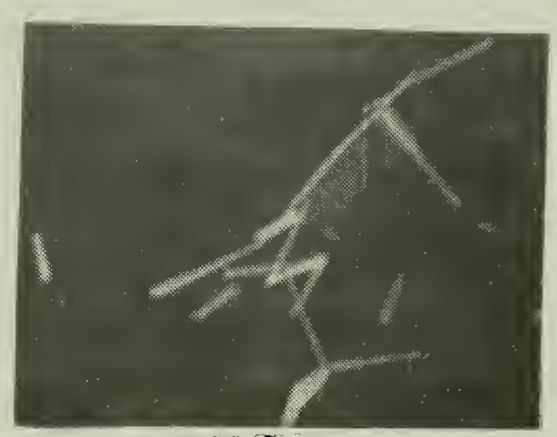

1275°C

1μ

SEM Photographs of ZnO Particles Produced at Temperatures from 1000°C to 1275°C

Figure 28

FIGURE 29

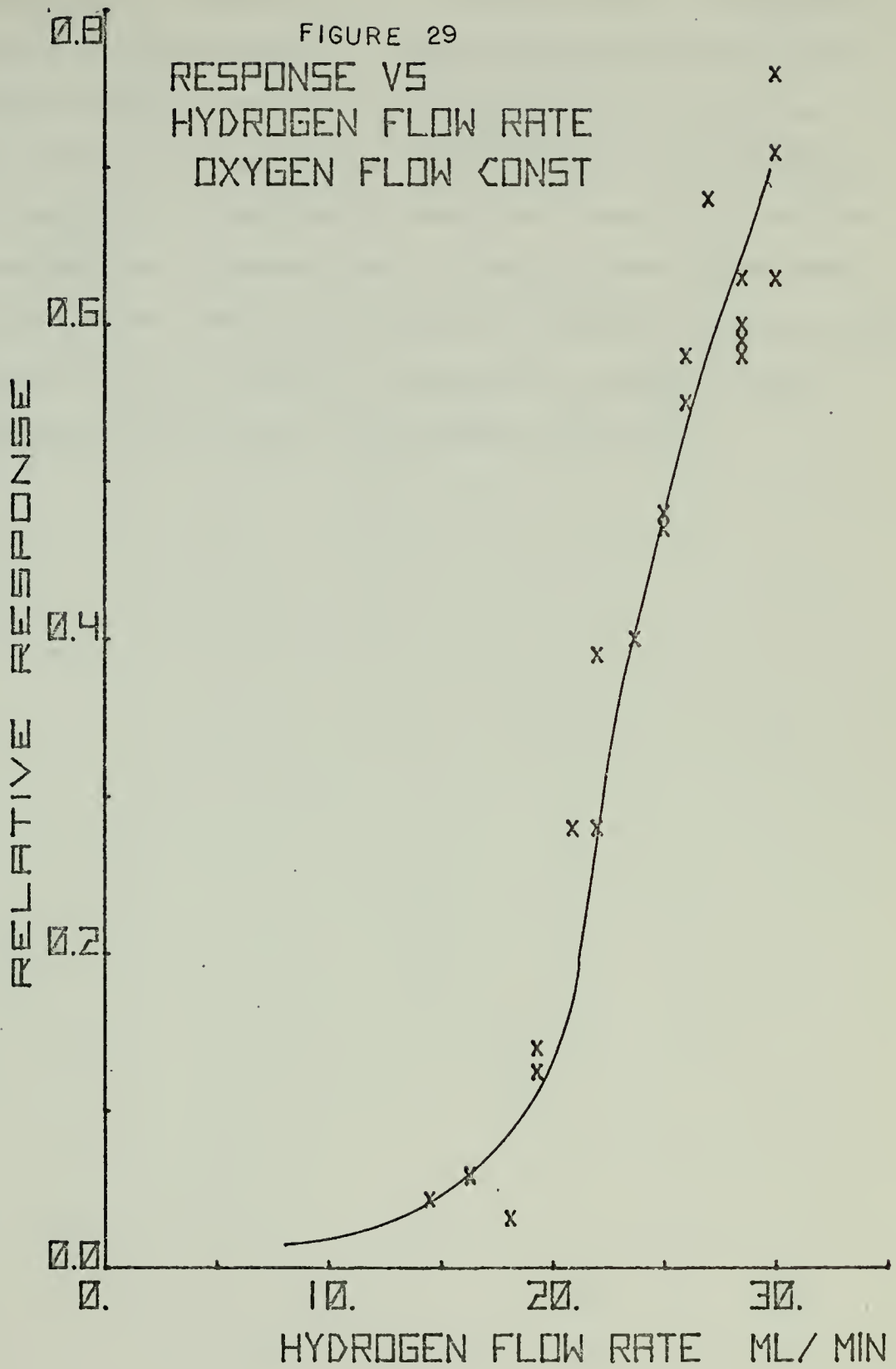
RESPONSE VS
HYDROGEN FLOW RATE
OXYGEN FLOW CONST
RELATIVE RESPONSE
0.8
0.6
0.4
0.2
0.0
0.
10.
20.
30.
HYDROGEN FLOW RATE ML/ MIN

at 85 ml/min. A 500 Volt, 17.2 Hz squarewave was applied to the cylindrical cavity. Figure 30 shows the dependence of the response under the same modulation conditions on oxygen flow rates holding the hydrogen flow rate constant at 27 ml/min. The maxima for each curve were used for the investigations; however, due to changing conditions among gas flow rates, ratios, and possible changes in the ZnO core, the flow had to be adjusted frequently to maintain some constancy in the normalizing response conditions.

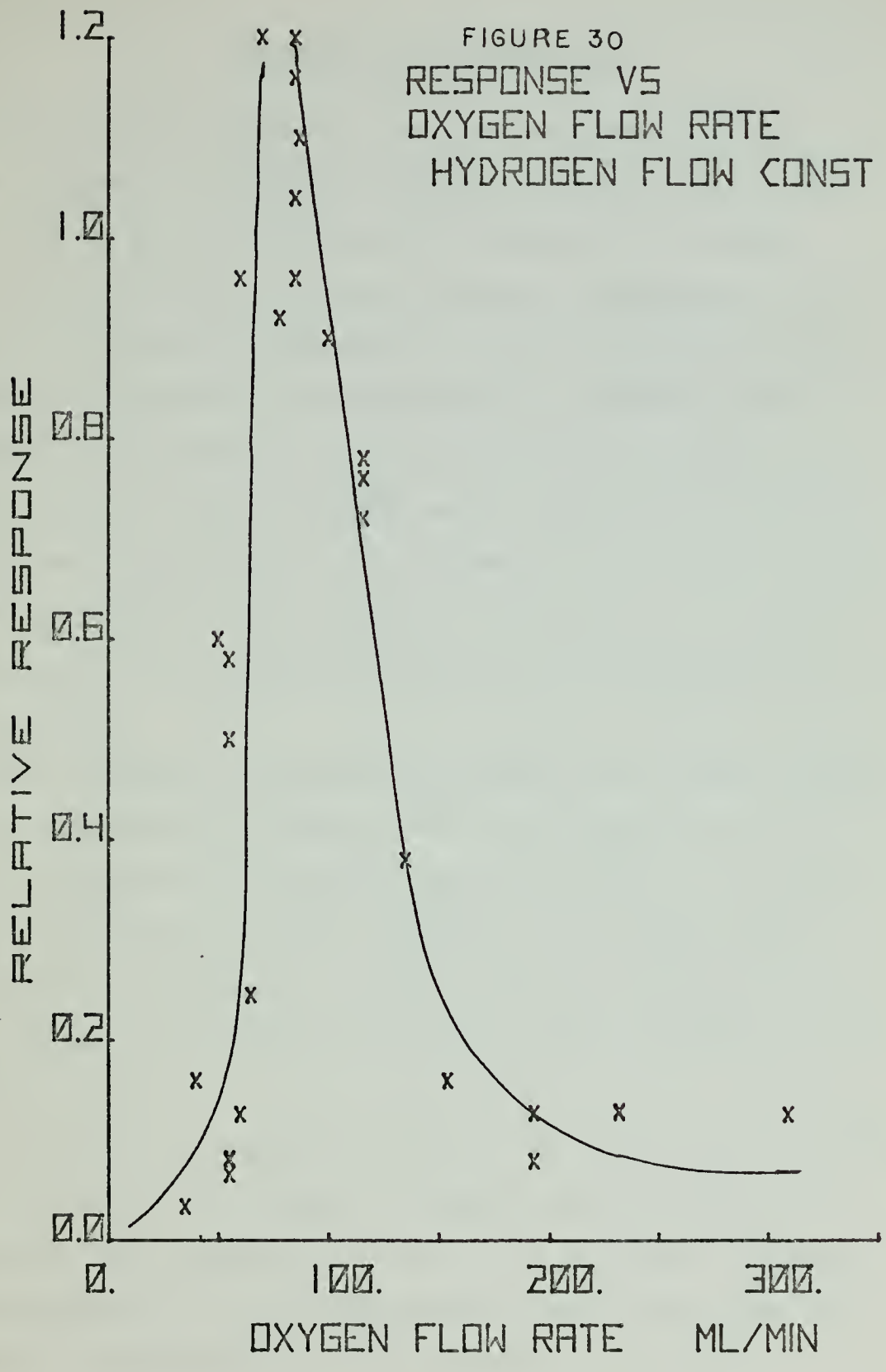
FIGURE 30
RESPONSE VS
OXYGEN FLOW RATE
HYDROGEN FLOW CONST
RELATIVE RESPONSE
1.2
1.0
0.8
0.6
0.4
0.2
0.0
0.
100.
200.
300.
OXYGEN FLOW RATE ML/MIN

V. SUMMARY AND CONCLUSIONS

Starting with dielectric methods developed for the investigation of molecular systems, a description has been developed to predict the dielectric behavior of larger (i.e., on the order of microns instead of angstroms) non-spherical particles suspended in a gas. The characteristic dielectric responses of saturation and relaxation were expanded. As stated in the Introduction, molecular saturation requires a field strength on the order of 10^5 Volts/cm and an oscillating field on the order of 10^{12} Hz for orientational relaxation. The predicted corresponding relaxation frequency for the suspended particles is on the order of 10 to 10^3 Hz.

This decrease in relaxation frequency is a direct result of the increased time required for the larger particles to reach an equilibrium alignment when subjected to a forcing field. The decrease in the strength of the field needed to produce saturation is a result of the increased polarizability associated with the larger particles and the larger aligning torque.

Utilizing the concepts developed, an experimental apparatus was developed to investigate non-spherical particulate suspensions. The apparatus consisted of a microwave resonant cavity designed to allow the introduction of suspended particles and the application of an electric field to force

particle alignment, and supporting equipment to detect and record the change in the cavity resonance as the suspended particles were aligned. To enhance the detectability of this response, modulation techniques were employed to modulate the particle alignment with respect to the resonant microwave E-field.

Different cavity geometries and methods of application of the electric field were investigated to find the cavity which would produce the most well defined response. A cylindrical coaxial cavity operating in the TE_{012} mode and resonant at 11.35 GHz was utilized to supply the necessary microwave resonance and aligning electric field application from inner rod to outer wall.

A lock-in amplifier and phase sensitive detector were employed to detect and amplify the presence of the modulation frequency in the detected cavity microwave output. Both in-phase and out-of-phase signals were recorded.

Saturation behavior was investigated utilizing two methods and a particulate suspension of zinc oxide particles. The first method investigated the direct cavity response. The second method involved the detection of the derivative cavity response. These two methods when compared show good correlation in the general response dependence on applied E-field strength and indicate that the particles produced exhibited saturation behavior for an applied electric field in excess of 400 to 500 Volts/cm.

Relaxation time (frequency) determinations were made by two methods also. The detected, in-phase, cavity response as the modulation frequency was increased indicated that the particles produced had an approximate relaxation time of 2.8×10^{-3} sec (56 Hz). To verify this value a Boxcar Integrator was utilized in place of the lock-in amplifier/ phase detector. The determined relaxation time for this method of 2.1×10^{-3} sec (75 Hz) further supports the developed methods.

Particle size determinations were also performed in conjunction with the saturation and relaxation investigations. Table V presents a comparison of determined particle sizes to collected particle sizes determined from scanning electron microscope (SEM) pictures of particles collected during the investigations. Particle size distribution was determined from the ratio of the detected in phase and out of phase response. The particles ranged from approximately 2 to 3.5 microns (μ) in length.

EXPERIMENT / VARIABLE	Saturation Investigation Direct	Saturation Investigation Deriv.	Relaxation Investigation	Boxcar Integrator
Collected particle size (SEM)	3.0μ	3.0μ	2.8μ	2.5μ
Experimental particle size	2.2μ	1.8μ	3μ	2.9μ

Comparison of Determined Particle Sizes for Investigations Performed (ZnO Particles)

Table V

Also investigated was a characterization of the dependence of the response to various zinc oxide production parameters. It was determined that the most intense response at a given modulation frequency and applied electric field strength was obtained when the zinc oxide suspension was produced at 1250° C and hydrogen and oxygen flow rates of 27 ml/min and 85 ml/min respectively.

The general shape of the response curves obtained from the different methods and the satisfactory agreement shown for the calculated size of the particles produced provide adequate evidence that the apparatus and experimental theory developed produce and describe the expected microwave dielectric response of non-spherical particles.

BIBLIOGRAPHY

1. Debye, P., Polar Molecules, Chemical Catalog, 1929.

2. Fröhlich, H., Theory of Dielectrics, 2nd ed., Oxford, 1958.

3. Smyth, C. P., Dielectric Behavior and Structure, p. 52, 95, McGraw-Hill, 1955.

4. Hill, N. E., and others, Dielectric Properties and Molecular Behaviors, p. 5, 158-162, Van Nostrand Reinhold, 1969.

5. Atlas, D., Kerker, M., Hitchfield, W., "Scattering and Attenuation by Non-Spherical Atmospheric Particles," Journal of Atmospheric and Terrestrial Physics, Vol. 3, p. 108-119, 1953.

6. Jones, A. R., "Scattering and Emission of Radiation by Clouds of Elongated Particles," Journal of Physics D: Applied Physics, Vol. 5, p. L1-L4, 1972.

7. Vogel, D. C., Circle, R. R., and Powell, R. S., "Experimental Arrangement for Comparison of the Optical and Physical Characteristics of Particulate Smokes," Review of Scientific Instruments, Vol. 38, no. 4, p. 499-501, April 1967.

8. Hidy, G. M. and Brock, J. R., International Reviews in Aerosol Physics and Chemistry, Vol. 2, Pergamon, 1971.

9. Montgomery, C. G., M.I.T. Radiation Laboratory Series, V. 11, p. 285-342, Boston Technical, 1964.

10. Ginzton, E. L., Microwave Measurements, p. 445-452, 484, McGraw-Hill, 1957.

11. Lax, B., and Button, K. J., Microwave Ferrite and Ferrimagnetics, p. 327-329, McGraw-Hill, 1962.

12. Pauling, L. and Wilson, E. B., Introduction to Quantum Mechanics, p. 185, McGraw-Hill, 1935.

13. Ditchfield, C. R., "The Effect of Coupling and Sample Properties on the Behavior of Microwave Cavities, Especially in Spectrometers and Masers," Royal Radar Establishment Technical Note No. 639, June 1958.

14. Carrington, A. and McLachlan, A. D., Introduction to Magnetic Resonance, p. 187-189, Harper & Row, 1967.

15. Happel, J. and Brenner, H., Low Reynolds Number Hydrodynamics, p. 215-232, Prentice-Hall, 1965.

16. Lamb, H., Hydrodynamics, p. 614-616, 6th ed., Dover, 1945.

17. Abramowitz, M. and Stegun, I. A., Handbook of Mathematical Functions with Formulas, Graphs, and Mathematical Tables, p. 930, U.S. Dept. of Commerce, NBS Appl. Math. Series 55, June 1964.

18. Dodson, E. M. and Savage, J. A., "Vapour Growth of Single-Crystal Zinc Oxide," Journal of Materials Science, Vol. 3, p. 19-25, 1958.

INITIAL DISTRIBUTION LIST

		No. Copies
1.	Defense Documentation Center Cameron Station Alexandria, Virginia 22314	2
2.	Library, Code 0212 Naval Postgraduate School Monterey, California 93940	2
3.	Professor W. M. Tolles, Code 61T1 Department of Physics and Chemistry Naval Postgraduate School Monterey, California 93940	3
4.	Professor G. E. Schacher, Code 61 Sq Department of Physics and Chemistry Naval Postgraduate School Monterey, California 93940	1
5.	Lt. Gerald W. Fritz, USN 1940 Paralta Avenue Seaside, California 93955	1
6.	Dr. William S. McEwan, Code 604 Naval Weapons Center China Lake, California 93555	1
7.	Department of Physics and Chemistry Library Naval Postgraduate School Monterey, California 93940	1

SECURITY CLASSIFICATION OF THIS PAGE (When Data Entered)

REPORT DOCUMENTATION PAGE

READ INSTRUCTIONS BEFORE COMPLETING FORM

1. REPORT NUMBER	2. GOVT ACCESSION NO. / 3. RECIPIENT'S CATALOG NUMBER
4. TITLE (and Subtitle): Microwave Dielectric Response of Non-Spherical Particles by Modulation Techniques	5. TYPE OF REPORT & PERIOD COVERED: Master's Thesis; March 1974
	6. PERFORMING ORG. REPORT NUMBER
7. AUTHOR(s): Gerald Wayne Fritz	8. CONTRACT OR GRANT NUMBER(s)
9. PERFORMING ORGANIZATION NAME AND ADDRESS: Naval Postgraduate School, Monterey, California 93940	10. PROGRAM ELEMENT, PROJECT, TASK AREA & WORK UNIT NUMBERS
11. CONTROLLING OFFICE NAME AND ADDRESS: Naval Postgraduate School, Monterey, California 93940	12. REPORT DATE: March 1974 13. NUMBER OF PAGES: 104
14. MONITORING AGENCY NAME & ADDRESS (if different from Controlling Office): Naval Postgraduate School, Monterey, California 93940	15. SECURITY CLASS. (of this report): Unclassified 15a. DECLASSIFICATION/DOWNGRADING SCHEDULE

16. DISTRIBUTION STATEMENT (of this Report)

Approved for public release; distribution unlimited.

17. DISTRIBUTION STATEMENT (of the abstract entered in Block 20, if different from Report)

18. SUPPLEMENTARY NOTES

19. KEY WORDS (Continue on reverse side if necessary and identify by block number)

Zinc Oxide	Microwave Properties
Dielectric Properties	Aerosols
Dielectric Relaxation	Particulates
Dielectric Modulation	Particulate Suspensions
Fourlings	Relaxation

20. ABSTRACT (Continue on reverse side if necessary and identify by block number)

A method was developed to investigate the dielectric response of non-spherical zinc oxide particles in a gaseous suspension. The method exploited a change in a microwave cavity resonance when the particles were aligned with respect to the microwave electric field. To enhance the detectability of this change, modulation techniques were employed for alignment and detection purposes.

A theory was devised to explain this method and experiments

DD FORM 1 JAN 73 1473 EDITION OF 1 NOV 65 IS OBSOLETE
S/N 0102-014-6601 |
(Page 1)

SECURITY CLASSIFICATION OF THIS PAGE (When Data Entered)

(19.) continued

Electric Field Modulation
Orientation Modulation
Polarization Saturation
Saturation

(20.) continued

were conducted, the results of which support this theory. Investigations with the zinc oxide particles produced in these experiments indicated that the particle response demonstrated saturation and that the particles are easily aligned in an electric field strength of several hundred Volts/cm. The zinc oxide particles produced showed a relaxation frequency of approximately 56 Hz and ranged in size from approximately 2.0 to 3.5 microns in length.

Thesis
F8945
c.1

Fritz

147574

Microwave dielectric response of non-spherical particles by modulation techniques.

Thesis
F8945
c.1

Fritz

147574

Microwave dielectric response of non-spherical particles by modulation techniques.

thesF8945
Microwave dielectric response of nonsphe
3 2768 001 90059 0
DUDLEY KNOX LIBRARY